PUBLISHED BY IOP PUBLISHING FOR SISSA

RECEIVED: *October 21, 2009*
REVISED: *November 22, 2009*
ACCEPTED: *December 21, 2009*
PUBLISHED: *March 19, 2010*

COMMISSIONING OF THE CMS EXPERIMENT WITH COSMIC RAYS

Alignment of the CMS silicon tracker during commissioning with cosmic rays

CMS Collaboration

ABSTRACT: The CMS silicon tracker, consisting of 1440 silicon pixel and 15 148 silicon strip detector modules, has been aligned using more than three million cosmic ray charged particles, with additional information from optical surveys. The positions of the modules were determined with respect to cosmic ray trajectories to an average precision of 3–4 microns RMS in the barrel and 3–14 microns RMS in the endcap in the most sensitive coordinate. The results have been validated by several studies, including laser beam cross-checks, track fit self-consistency, track residuals in overlapping module regions, and track parameter resolution, and are compared with predictions obtained from simulation. Correlated systematic effects have been investigated. The track parameter resolutions obtained with this alignment are close to the design performance.

KEYWORDS: Large detector systems for particle and astroparticle physics; Particle tracking detectors (Solid-state detectors)

ARXIV EPRINT: 0910.2505

doi:10.1088/1748-0221/5/03/T03009

2010 JINST 5 T03009

Contents

2010 JINST 5 T03009

1 Introduction

The main goal of the CMS experiment [1] is to explore physics at the TeV energy scale exploiting the proton-proton collisions delivered by the Large Hadron Collider (LHC) [2]. The CMS silicon tracking detector (tracker) [3, 4] consists of 1440 silicon pixel and 15 148 silicon strip detector modules and is located, together with the electromagnetic and hadronic calorimeters, inside a superconducting solenoidal magnet operating at a field of 3.8 T. Outside of the solenoid, the muon system is used both for triggering on muons and reconstructing their trajectories.

The aim of the tracker is to measure the trajectories of charged particles (tracks) with excellent momentum, angle, and position resolution, and with high pattern recognition efficiency [5]. Precise determination of the position of all silicon modules is a challenging task and one of the critical aspects for achieving the design track parameter resolutions. In the context of alignment, *position* is used throughout this paper to refer both to the location of the center point of active areas on

modules and to the orientation of active areas. The hit position resolution is in the range 10 to 30 μm and therefore the alignment precision should be better than 10 μm to achieve optimal track parameter resolution. Simulation studies based on the design (ideal) tracker geometry imply an impact parameter resolution of about 15 μm and a transverse momentum (p_T) resolution of about 1.5% for 100 GeV/c muons.

The CMS collaboration conducted a month-long data-taking exercise known as the Cosmic Run At Four Tesla (CRAFT) during October-November 2008 with the goal of commissioning the experiment for extended data-taking [6]. With all installed detector systems participating, CMS recorded 270 million cosmic-ray-triggered events with the solenoid at its nominal axial field strength of 3.8 T. However, only a few percent of those events had cosmic rays traversing the tracker volume. Prior to CRAFT and during the final installation phase of the experiment, a series of commissioning exercises to record cosmic ray events took place with the solenoid turned off from May to September 2008. The tracker was included only at the later stages of those runs and a smaller number of cosmic ray events with the tracker participation were recorded compared with CRAFT. The operating temperature of the tracker during the CRAFT data-taking period was stable at around room temperature. Excellent performance of the tracking system has been achieved with both the silicon strip [7] and silicon pixel [8] components.

In this paper, the measurement of detector module positions for the full tracker from alignment analysis with cosmic ray particles, optical survey information, and the Laser Alignment System (LAS) is presented. This work builds on the experience with the alignment of about 15% of the CMS silicon strip tracker during stand-alone commissioning [9]. Significant improvements have been introduced. Inclusion of the pixel detector and of the full strip tracker made the first alignment of the whole CMS tracker possible. The magnetic field allowed estimates of the multiple scattering effects on a track-by-track basis. The data taken with the solenoid turned off were used in this analysis to cross-check the field-on data in a small number of cases. Significantly more tracks in a single stable configuration improved statistical precision. Two complementary statistical alignment algorithms, a global and a local iterative method, were applied to the data. Although both algorithms had been used previously during stand-alone commissioning, further improvements have been introduced, such as inclusion of survey data together with tracks. Results from the alignment studies have been compared extensively with detailed Monte Carlo (MC) simulations of the detector.

This paper is structured as follows: in section 2, the tracker layout and coordinate systems are introduced. Section 3 summarizes the optical survey measurements. In section 4, the track reconstruction and alignment algorithms are described and their application to data is explained. Results are presented in section 5.

2 Tracker layout and the coordinate systems

CMS uses a right-handed coordinate system, with the origin at the nominal collision point, the x-axis pointing to the center of the LHC, the y-axis pointing up (perpendicular to the LHC plane), and the z-axis along the anticlockwise-beam direction. The polar angle (θ) is measured from the positive z-axis and the azimuthal angle (ϕ) is measured from the positive x-axis in the x-y plane, whereas the radius (r) denotes the distance from the z-axis.

2010 JINST 5 T03009

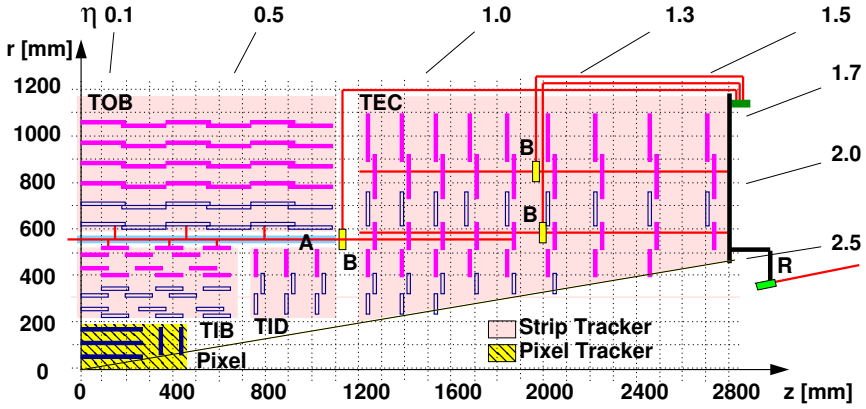

Figure 1. A quarter of the CMS silicon tracker in an rz view. Single-sided silicon strip module positions are indicated as solid light (purple) lines, double-sided strip modules as open (blue) lines, and pixel modules as solid dark (blue) lines. Also shown are the paths of the laser rays (R), the beam splitters (B), and the alignment tubes (A) of the Laser Alignment System.

The CMS tracker consists of a silicon pixel detector and a silicon strip detector (figure 1). The silicon pixel detector is composed of two sub-detectors, the barrel (BPIX) and the two endcaps in the forward regions (FPIX). The pixel modules provide two-dimensional measurements of the hit position in the module planes, which effectively translate into three-dimensional measurements in space. The silicon strip detector is composed of four sub-detectors: the Tracker Inner and Outer Barrels (TIB and TOB), the Tracker Inner Disks (TID), and the Tracker Endcaps (TEC). All sub-detectors are concentrically arranged around the nominal beam axis. The two inner layers of both the TIB and TOB, the two inner rings of the TID, and the first, second, and fifth rings of the TEC are equipped with double-sided modules; all other positions have single-sided modules. Single-sided modules provide $r\phi$ measurements in the barrel and ϕ measurements in the endcaps. Double-sided modules are made of a pair of single-sided strip modules, one $r\phi$ and one stereo module in the barrel, and one ϕ and one stereo module in the endcaps, precisely mounted back-to-back, with the stereo module sensors tilted by 100 mrad. For simplicity, we refer to both $r\phi$ and ϕ modules as $r\phi$ in the rest of the paper.

In the barrel region, modules are arranged in linear structures parallel to the z-axis, such as ladders in the BPIX, strings in the TIB, and rods in the TOB. The endcaps are composed of disks, which in turn contain wedge-shaped structures covering a narrow ϕ region, such as blades in the FPIX and petals in the TEC. The BPIX and the TIB are composed of two half-barrel structures, separated along the $x = 0$ plane for the BPIX and the $z = 0$ plane for the TIB.

A local right-handed coordinate system is defined for each module with the origin at the geometric center of the active area of the module. As illustrated in figure 2, the u-axis is defined along the more precisely measured coordinate of the module (typically along the azimuthal direction in the global system), the v-axis orthogonal to the u-axis and in the module plane, pointing away from the readout electronics, and the w-axis normal to the module plane. When double-sided modules are considered as a single entity, the coordinate system is referenced to the $r\phi$ module. For the pixel system, u is always orthogonal to the magnetic field, that is in global $r\phi$ direction in the BPIX

2010 JINST 5 T03009

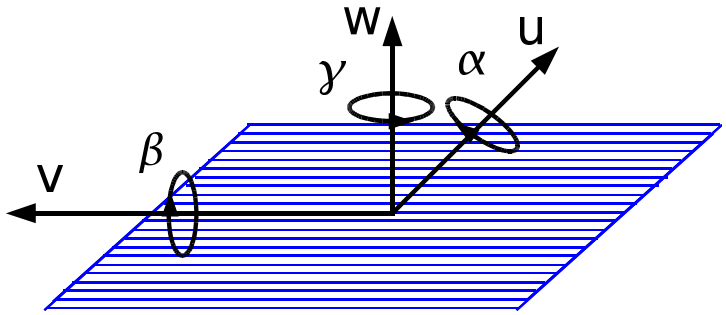

Figure 2. Illustration of the module local coordinates u, v, w and the corresponding rotations α, β, γ for a single-sided strip module.

and in the radial direction in the FPIX. The v coordinate is perpendicular to u in the sensor plane, that is along global z in the BPIX and at a small angle to the global $r\phi$ direction in the FPIX. The angles α, β, and γ indicate rotations about the u, v, and w axes, respectively.

In addition, local u' and v' coordinates are defined such that they are parallel to u and v, but the direction is always chosen to be in positive ϕ, z, or r directions, irrespective of the orientation of the local coordinate system. For the TID and TEC wedge-shaped sensors, where the topology of the strips is radial, the u'- and v'-axes change direction across the sensor such that v' is always directed along the strips and therefore u' corresponds to the global $r\phi$-coordinate.

3 Optical survey measurements

Optical surveys taken during module construction and integration provide initial alignment parameters for many of the modules. Additionally, the survey information was used as a constraint in the alignment procedure, as will be described in section 4.1.

Coordinate Measuring Machine (CMM) data and photogrammetry have been used for the optical survey of the tracker components. While the former were used for measurements of the active elements, the latter were used for the alignment of larger structures. For the inner strip detectors (TIB and TID), both module-level and high-level structure information were used in the analysis. For the outer strip detectors (TOB and TEC), module-level survey data were used only as a conformance criterion during construction, while survey information from high-level structures was used in the analysis. More information on the strip detector surveys can be found in ref. [9].

Detailed optical surveys of the pixel endcap detectors were performed as part of the construction process. First, module positions were measured within a panel, which contains three or four modules. Then the positions of modules were also measured on a half-disk, where 12 panels are placed on each side. Eight fiducial points were measured on the active area of each module, allowing a position measurement precision of about one micron. Some of the module fiducial points were partially obscured by other modules when mounted on a half-disk and thus could not be measured. Good reproducibility of module measurements within a panel was found in the two configurations, allowing an estimate of survey precision. Measurements of the two sides of the half-disk were connected through a touch-probe, which related positions of the touch-probe targets previously measured with CMMs. This also related measurements from the front and the back

2010 JINST 5 T03009

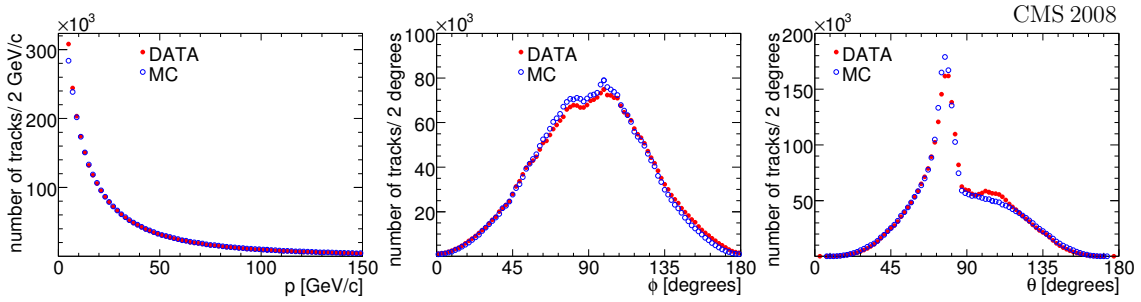

Figure 3. Momentum (left), azimuthal angle (middle), and polar angle (right) spectra of cosmic muons reconstructed in the CMS tracker volume based on the selection criteria described in the text. The solid (red) circles represent the cosmic ray data whereas the open (blue) circles come from a MC simulation. The vertical cosmic ray tracks correspond approximately to $\phi = \theta = 90^\circ$.

panels of blades. Finally, half-disks were placed in the half-cylinders, which were then inserted in the pixel detector volume. Half-disk and half-cylinder positions were measured with photogrammetry and were related to the positions of the active elements through photo targets, which had been previously measured with CMMs.

In the barrel pixel detector, only two-dimensional measurements of the module positions within a ladder were performed. High-resolution digital images of four nearby fiducial points in neighboring modules were taken. A precision of 2 μm was achieved for longitudinal positions of the modules within a ladder, allowing, in particular, a tight constraint on the z-scale. The relative position of nearby ladders in the half-shells were also surveyed with similar two-dimensional measurements, but were not used in this analysis.

4 Track-based alignment

The goal of the track-based alignment procedures is to determine the module positions from a large sample of reconstructed charged particle trajectories. Each trajectory is built from charge depositions ("hits") on individual detectors, assuming a piece-wise helical track model, incorporating effects from multiple scattering and energy loss. The "Combinatorial Track Finder" (CTF) track algorithm [7] was used to reconstruct the cosmic muon trajectories. The result is a set of track parameters. Five track parameters describe the helical trajectory of a track at the point closest to the nominal interaction point: distance of closest approach in the transverse d_{xy} and longitudinal d_z directions, track azimuthal angle ϕ, track polar angle θ, and transverse momentum p_T.

The momentum and angular spectra of cosmic muons reconstructed in the CMS tracker volume are shown in figure 3, where good agreement with MC simulation [10] is observed. These track parameters are defined at the point of closest approach to the CMS nominal interaction point and the absolute value of the ϕ angle is shown, considering all particles traversing CMS from top to bottom. The aligned tracker geometry was used in track reconstruction. The asymmetry about $\phi = 90^\circ$ is due to the excess of positive over negative cosmic ray particles entering CMS and the bending of charged tracks in the magnetic field of the solenoid. Positively charged cosmic rays tend to peak just above 90° whereas negatively charged cosmic rays tend to peak just below 90°.

2010 JINST 5 T03009

The asymmetry about $\theta = 90^\circ$ is mainly due to the asymmetric location of the cavern shaft. Tracks were selected according to the following criteria. Each track was required to consist of at least eight hits with a signal-to-noise ratio larger than 12 in the silicon strip modules or a probability of the pixel hit matching the template shape [11] of at least 0.001 (0.01) in the local u (v) direction. Hits were also rejected if the track angle relative to the local uv plane was less than 20°. In addition, two hits were required to be on either pixel or double-sided strip modules, allowing a precise measurement of the polar angle θ. The particle momentum had to be greater than 4 GeV/c, and the χ^2 per degree of freedom of the track fit, χ^2/ndf, had to be less than 6.0. Outlying hits with large normalized residuals were removed. In total, about 3.2 million tracks were selected for alignment, out of which about 110 000 had at least one pixel hit.

The track reconstruction used the Alignment Position Errors (APE), the estimated uncertainty on the module position in the three global coordinates, which were added in quadrature to the hit errors during the pattern recognition and track fitting procedure. This allowed efficient track reconstruction in the presence of misalignment and a correct pull distribution of track parameters. The determination of APEs is described in section 5.1. The APE values used for the initial track reconstruction before alignment analysis were set to large values as they had to account for possible large displacements of the entire sub-detectors while still guaranteeing an efficient track-hit association.

4.1 Alignment algorithms

The alignment is an optimization problem that can be formulated in the context of linear least squares. Module position corrections ("alignment parameters") $\mathbf{p}$ are determined by minimizing an objective function

$$\chi^2(\mathbf{p},\mathbf{q}) = \sum_{j}^{\text{tracks}} \sum_{i}^{\text{hits}} \mathbf{r}_{ij}^T(\mathbf{p},\mathbf{q}_j)\mathbf{V}_{ij}^{-1}\mathbf{r}_{ij}(\mathbf{p},\mathbf{q}_j)\,, \tag{4.1}$$

which can be expressed as the sum over all hits i on all tracks j and track parameters $\mathbf{q}_j$, assuming negligible correlations between hits. Track residuals $\mathbf{r}_{ij} = \mathbf{m}_{ij} - \mathbf{f}_{ij}(\mathbf{p},\mathbf{q}_j)$ are defined as the difference between the measured hit position $\mathbf{m}_{ij}$ and the trajectory impact point $\mathbf{f}_{ij}$, both of which are given in the module local coordinate system. The residuals are either one- or two-dimensional vectors, depending on the type of module, and $\mathbf{V}_{ij}$ is either the squared error or the covariance matrix in case of one- or two-dimensional residuals, respectively.

Two statistical methods were employed to solve the alignment problem. Both of them were previously applied to the CMS silicon strip tracker alignment during stand-alone commissioning [9]. The global alignment algorithm ("Millepede II") [12] minimizes the χ^2 function in eq. (4.1) by taking into account track and alignment parameters simultaneously. This algorithm has also been previously used in simulation studies of the CMS tracker [13]. Since only the n alignment parameters $\mathbf{p}$ are of interest, the problem is reduced to the solution of a matrix equation of size n. The value of n is of the order of 10^5 for six degrees of freedom of 16 588 modules. The covariance matrix $\mathbf{V}_{ij}$ is approximated by a diagonal matrix with uncertainties σ_{ij} for uncorrelated hit measurements $\mathbf{m}_{ij}$ of the track j. Given reasonable starting values, $\mathbf{p}_0$ and $\mathbf{q}_{j0}$, the track model prediction $\mathbf{f}_{ij}(\mathbf{p},\mathbf{q}_j)$ can be linearized. Since angular corrections are small, the linearized problem is a good approximation for alignment.

2010 JINST 5 T03009

The local iterative algorithm ("Hits and Impact Points") [14] approximates eq. (4.1) by assuming no track parameter $\mathbf{q}$ dependence and therefore ignores correlations between alignment parameters for different modules in one iteration. The trajectory impact point $\mathbf{f}_{\alpha j}$ is recalculated for each hit, removing the hit under consideration from the track fit. The track parameters and correlations between different modules are taken into account through iterations of the minimization procedure and refitting the tracks with new alignment constants after each iteration. The number of iterations is determined empirically. This approach allows a simplification of the formalism and leads to a solution of the six-dimensional matrix equation for the six alignment parameters of each module in each iteration.

The local iterative algorithm permits the inclusion of survey measurements in the formalism of eq. (4.1), as described in ref. [15]. This leads to an additional term in the objective function to be minimized independently for each module in a given iteration:

$$\chi^2_m(\mathbf{p}) = \sum_i^{\text{hits}} \mathbf{r}_i^T(\mathbf{p}) \mathbf{V}_i^{-1} \mathbf{r}_i(\mathbf{p}) + \sum_j^{\text{survey}} \mathbf{r}_{*j}^T(\mathbf{p}) \mathbf{V}_{*j}^{-1} \mathbf{r}_{*j}(\mathbf{p}) \,, \tag{4.2}$$

where the original formulation has been modified to include survey information from the k hierarchial levels for each sub-detector. The track residuals $\mathbf{r}_i(\mathbf{p})$ do not have explicit dependence on track parameters and enter the sum over hits in a given module m. The six-dimensional survey residuals $\mathbf{r}_{*j}$ are defined as the difference between the reference and the current sensor position. The survey measurement covariance matrix $\mathbf{V}_{*j}$ reflects both the survey precision and additional uncertainties due to changes in the detector. These errors can be configured differently for different hierarchy levels and for the degrees of freedom that should be stable, such as the longitudinal direction in a barrel ladder, and those which may change more with time.

The local iterative method uses the full implementation of the Kalman filter track reconstruction algorithm adopted in CMS [7]. It requires a large number of iterations and large computing resources to refit the tracks in each iteration. The global method, instead, allows the determination of alignment parameters, properly accounting for the correlations among them, in a single step. However, the global method does not take into account the effects of material in the tracker and assumes a simple helical trajectory for charged particles. The method also requires a large amount of computer memory and the application of advanced techniques [12] for solving eq. (4.1). Each of the two alignment algorithms was used to obtain module positions independently and a comparison of results between the two complementary approaches was part of the validation of the tracker alignment procedure. After verifying that the two methods yielded consistent results, the final results were obtained by applying the two algorithms in sequence in order to take advantage of their complementary strengths.

4.2 Alignment strategy

Single-sided silicon strip modules provide only a one-dimensional measurement in the module plane, along the local u-coordinate, which effectively translates into a two-dimensional measurement in space. The v-coordinate is only known to be within the module boundaries, with precision not sufficient for track reconstruction requirements. However, the information from the $r\phi$ and stereo modules in a double-sided module is combined into a two-dimensional measurement in the combined module plane in both u and v for the pattern recognition phase.

2010 JINST 5 T03009

Due to the 100 mrad stereo angle between the $r\phi$ and stereo modules, though, a small displacement in u is equivalent to a ten times larger displacement in v. Given comparable mounting precision of modules in u and v, a smaller u displacement is much more likely than a larger v displacement. In fact, it was found from the data after several attempts at alignment of double-sided modules in v, that parameters much larger than the known assembly accuracy were obtained. Whenever possible, the two single-sided components of a double-sided module were aligned separately, but only in the most precise coordinates. The relative alignment of the two sides was found to be consistent with assembly tolerance and at the same time improved track residuals significantly. This fact and the hierarchical structure of the tracker led to multi-step strategies for both alignment methods.

4.3 Alignment with the global method

The first step of the global method aligns the highest-level structures (half-barrels, endcaps) with all six degrees of freedom together with all module units, including $r\phi$ and stereo strip modules in a double-sided module, with the most sensitive degrees of freedom each (u, w, γ, and for pixel modules also v). The detector design geometry was chosen as a starting point. A limitation of 46 340 parameters in the program used led to selection criteria for modules to be aligned of more than 25 hits per pixel module and more than 425 hits per strip module. This resulted in the alignment of about 90% of all modules.

In the second step all modules (all double-sided or single-sided strip modules with more than 150 hits and all pixel modules with more than 25 hits) were aligned in the TIB in $u, w, \alpha, \beta, \gamma$; in the pixel system in u, v, w, γ; and in u, w, γ elsewhere. Compared to the previous step, this recovered the remaining 10% of the modules and allowed more degrees of freedom for the TIB, which had larger assembly tolerance, but did not allow independent alignment of the $r\phi$ and stereo modules within double-sided combinations. No alignment of α and β was performed in the TOB due to its higher mounting accuracy, and in the TID and TEC, since they were less often traversed by cosmic ray tracks.

The third step was designed to recover lost correlations between the first two steps and had the same configuration as the first step, but the minimum number of hits in the strip modules was increased to 450 with respect to 425 used in the first step.

4.4 Alignment with the local method

Module positions as determined from optical surveys were used as the starting point in the local method. The difference of the starting geometry to that of the global method was motivated by the use of survey information in the minimization procedure, as described in section 4.1. However, for both methods the initial geometry did not affect the results significantly. The alignment with the local algorithm started with the large structures and then proceeded in order of increasing granularity down to the module units in order to speed up convergence. The small fraction (4%) of tracks passing through the pixel detector suggested a modified approach in which the silicon strip modules were first aligned without pixel information. The hits from the structures not yet aligned were excluded from the track fit. The APE values were set high at the beginning of the alignment process (several hundreds of microns depending on the sub-detector), and were progressively re-

2010 JINST 5 T03009

duced to a few tens of microns in subsequent alignment steps. The values of the APEs were kept fixed within each alignment step.

The alignment with the local method was carried out in six steps. In the first step (15 iterations), the half-barrels of BPIX, TIB, and TOB were aligned as rigid bodies with four degrees of freedom (u,v,w,γ). In order to have a better sensitivity along the global z-direction, only tracks passing through the pixel barrel system were used. In the second step (15 iterations), the endcaps of the FPIX, TID, and TEC were aligned in the same four degrees of freedom. The third alignment step (30 iterations) moved the strip modules (treating double-sided modules as rigid bodies) in all six degrees of freedom. Data from the optical survey measurements (or design geometry if no survey information was available) were used according to eq. (4.2). The information on the module positions within a higher-hierarchy structure, for example within a string of TIB, was used in the χ^2 minimization. This proved to be useful for both limiting the movement of modules in poorly constrained degrees of freedom and aligning modules that had fewer than the required number of hits. In the fourth step (30 iterations), the strip module units (treating $r\phi$ and stereo strip modules in a double-sided module independently) with at least 50 hits were aligned in three degrees of freedom (u, w, γ). In step five (15 iterations), the ladders of the pixel detector were aligned in six degrees of freedom. Finally in the sixth step (15 iterations), the pixel modules with at least 30 hits were aligned in all six degrees of freedom.

After every step the alignment parameters were checked for convergence. Fewer than 20 modules failed to converge since they were moved to implausible positions by the algorithm. The alignment parameters for these modules were left at the survey values. It was found that in some cases the basic procedure needed to be applied a second time in order to improve the convergence for the alignment of the large-scale structures. However, as will be discussed in the next section, the final alignment results were derived from a sequential approach involving both the global and the local method, and for this reason the local method was limited to a single set of steps.

4.5 Alignment with the combined method

The strength of the global method is solving effectively the global correlations, while for the local method it is that the same track fit is used as in the standard CMS reconstruction, and that survey information can easily be incorporated thus allowing for alignment with more degrees of freedom. In order to take advantage of both methods, the final alignment parameters were produced starting from the output of the global method analysis described in section 4.3, then further aligning the tracker with the local method presented in section 4.4.

The alignment strategy adopted by the local algorithm was modified to exploit the already good starting position of the modules provided by the global method. The APEs were kept fixed at 10 μm in the barrels and 30 μm in the endcaps, similar to those described in section 5.1. In the first step of the local method (30 iterations), all strip modules (treating double-sided modules as rigid bodies) were aligned in six degrees of freedom using track and survey information. In the second step (20 iterations), the strip module units (treating $r\phi$ and stereo strip modules in a double-sided module independently) were aligned in three degrees of freedom (u,w,γ). Pixel modules were not aligned in the first two steps, although pixel hits were included in the track fit. Finally, in the last step (20 iterations), the pixel modules were aligned in six degrees of freedom. Modules for which the fit did not converge were left at the position obtained by the global algorithm.

2010 JINST 5 T03009

5 Results and validation

The alignment analysis was performed after the proper calibration of both the strip and pixel detectors [7, 8]. In particular, an appropriate Lorentz angle calibration was applied. A Lorentz angle miscalibration would result in a systematic shift of the effective charge collection position, in the same u-direction for all the modules with the same relative orientation between the solenoid and the drift field. Since this would appear as an effective shift of the module, it would not be evident if corrected for by the alignment. Therefore, for validation purpose only, alignment results were checked with the data collected both with 0 T and with 3.8 T solenoid fields. The precision achieved in the alignment analysis is such that there should be clear evidence for a Lorentz angle miscalibration with an effective shift of only a few microns. In fact, good agreement with the Lorentz angle calibration [7] was found.

Several approaches were employed to validate the alignment results. The low-level quantities that were used in the χ^2 minimization, such as residuals and the χ^2/ndf of the tracks, were monitored. Given the limited size of the alignment track sample, it was used both for alignment and validation. In addition, a high-level validation analysis was performed to monitor the track parameter resolution. Moreover, techniques for comparing positions of modules within differently derived geometries, described in sections 5.5 and 5.6, allowed a better understanding of the alignment performance.

5.1 Calibration of alignment position errors

In the track refit the APEs for each hit were assumed to be the same in the three spatial directions. For an alignment performed using cosmic ray tracks, the precision of the alignment varies within a given sub-detector because of the different illumination of modules due to their orientation relative to cosmic rays. The radius of the sphere representing the APE for each module, r_{sphere}, was therefore taken to be $r_{\text{sphere}} = r_0/\sqrt{N_{\text{entries}}}$, where N_{entries} represents the number of hits in a module. The value of r_0 was chosen in order to have the Gaussian standard deviation of the distribution of the residuals normalized to their error approximately equal to one in the symmetric interval covering 95% of the distribution. In the TIB and TOB, a common r_0 value was defined for each layer and separately for the $r\phi$ and stereo components of the double-sided layers. Elsewhere the value of r_0 was defined at the sub-detector level. The values of r_{sphere} were restricted to reasonable values, especially in the case of small or zero N_{entries}, where a precision compatible with survey and assembly data was used. APEs were calibrated using the set of alignment parameters obtained from the combined method. Examples of the distribution of the normalized residuals after the calibration of the APEs are shown in figure 4.

5.2 Track fit quality and hit residuals

All tracks used in the validation procedure were refitted with APEs corresponding to the alignment parameters obtained with the combined method. The loose track selection described in section 4 was applied. To avoid a bias in the determination of the hit residuals, the track prediction was calculated without information from the hit under consideration. The track χ^2/ndf distribution is shown in figure 5. The hit residuals in the u' and v' directions are shown in figure 6. The hit residual width is dominated by two effects other than alignment: track extrapolation uncertainties due to

2010 JINST 5 T03009

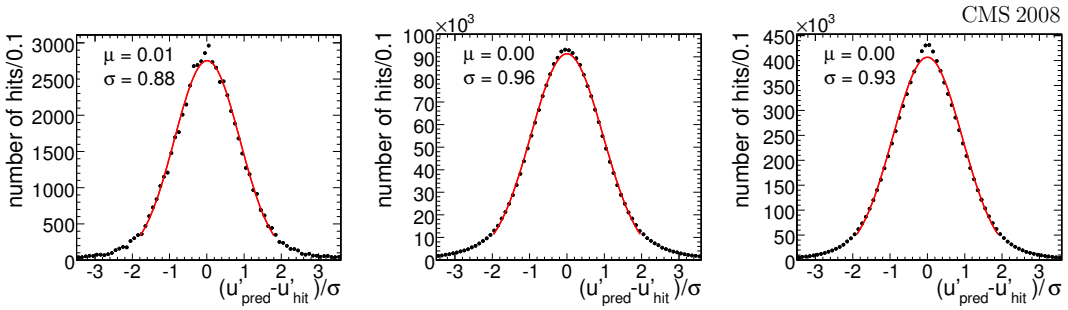

Figure 4. Distributions of normalized track residuals after the APE calibration procedure: BPIX (left), TIB (center), and TOB (right). Solid lines represent the results of Gaussian fits and the fit mean and sigma values are given within the plots. The alignment obtained from the combined method was used.

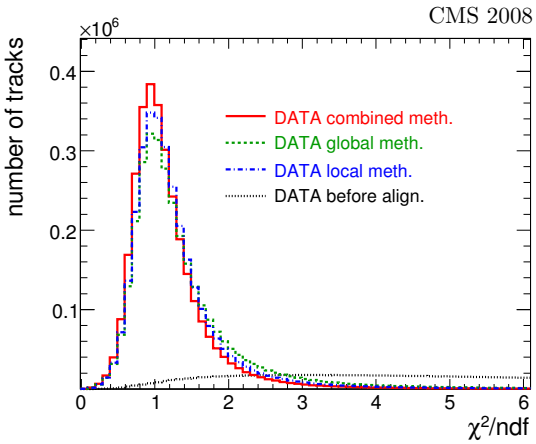

Figure 5. Distributions of the χ^2/ndf of the tracks before alignment (dotted line) and after alignment with the local (dashed-dotted line), global (dashed line), and combined (solid line) methods.

multiple scattering and hit position reconstruction uncertainties. Both of these effects are random, while misalignment leads to systematic shifts of the residuals. For this reason, the distribution of the median of the residuals (DMR) is taken as the most appropriate measure of alignment. Median distributions are shown in figure 7 and the corresponding RMS values of these distributions are given in table 1.

To check the statistical precision of track-based alignment a MC simulation was performed in which module positions from the combined method obtained with data were used as the starting geometry in the MC alignment procedure. This approach in MC effectively models the situation in data prior to and during the alignment. The resulting DMRs are also shown in figure 7 and the RMS values listed in table 1. For comparison, the distributions obtained from the ideal MC simulation are presented in figure 7 as well.

The middle columns of table 1 reflect different stages of alignment: the initial situation with no alignment, alignment with tracks using the global and local methods, and finally with the combined method. Table 1 also includes results from MC simulations based on combined and ideal geometries. For the 2D pixel detectors both u' and v' coordinate measurements are quoted. Over-

2010 JINST 5 T03009

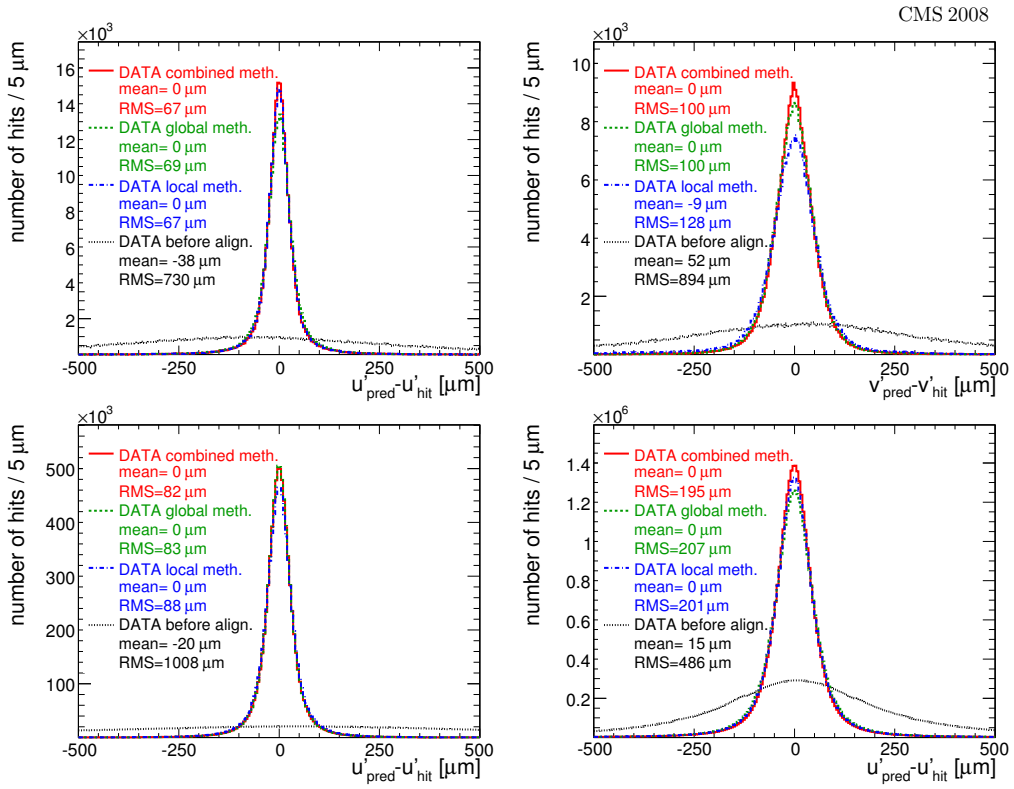

Figure 6. Track residuals, shown for BPIX (top left u', top right v'), TIB (bottom left), and TOB (bottom right). The four lines correspond to positions before alignment (dotted lines) and after alignment with the global (dashed lines), local (dot-dashed lines), and combined methods (solid lines).

all, there is significant improvement in the track reconstruction going from the geometry without any alignment, to the alignment using tracks with the local and the global method, and finally to the combined result. With respect to cosmic ray trajectories, the module positions were determined to an average precision of 3–4 μm RMS in the barrel and 3–14 μm RMS in the endcaps in the most sensitive coordinate. These values are in agreement with the expected statistical precision as determined using simulated events. They are also comparable to values obtained from a MC simulation based on the ideal detector geometry.

5.3 Residuals in overlapping module regions

A further method to monitor and validate the results of the alignment is to use the hits from tracks passing through regions where modules overlap within a layer of the tracker. This method, described in detail in ref. [16], is also used to measure the hit resolution of the sensors [7]. In this method, the difference in residual values for the two measurements in the overlapping modules is compared, once the hits in the layer under consideration are removed from the track fit. The proximity of the hits reduces the amount of material between the two hits and minimizes the uncertainties on the predicted positions associated with track propagation. Deviations between

2010 JINST 5 T03009

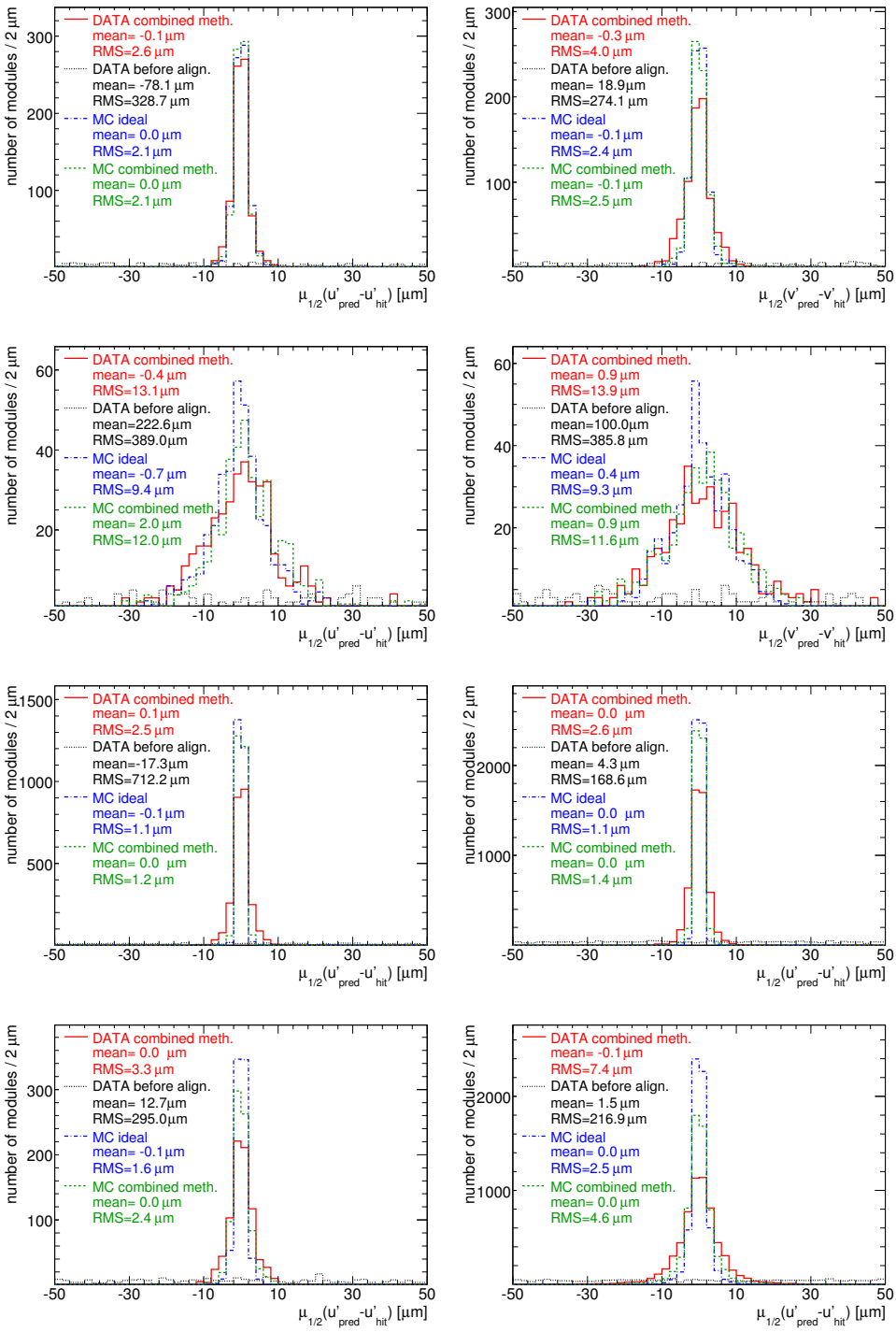

Figure 7. Distribution of $\mu_{1/2}$, the median of the residuals, for modules with more than 30 hits, shown for BPIX (top left u', top right v'), FPIX (second row left u', second row right v'), TIB (third row left), TOB (third row right), TID (bottom left), and TEC (bottom right). Shown are distributions before alignment (black dotted), after alignment with the combined method (red solid), combined method MC (green dashed), and ideal MC (blue dash-dotted).

2010 JINST 5 T03009

Table 1. RMS of the distribution of the median of the residuals (DMR) in the u' and v' local coordinates for modules with more than 30 hits. The number of these modules compared to the total number of modules is stated in the last column. Four geometries are considered: those obtained with the three methods discussed in the text and the geometry before alignment. Results from simulations based on the combined alignment and ideal geometries are shown for comparison.

	before [μm]	global [μm]	local [μm]	combined [μm]	combined MC [μm]	ideal MC [μm]	modules >30 hits
BPIX (u')	328.7	7.5	3.0	2.6	2.1	2.1	757/768
BPIX (v')	274.1	6.9	13.4	4.0	2.5	2.4	
FPIX (u')	389.0	23.5	26.5	13.1	12.0	9.4	393/672
FPIX (v')	385.8	20.0	23.9	13.9	11.6	9.3	
TIB (u')	712.2	4.9	7.1	2.5	1.2	1.1	2623/2724
TOB (u')	168.6	5.7	3.5	2.6	1.4	1.1	5129/5208
TID (u')	295.0	7.0	6.9	3.3	2.4	1.6	807/816
TEC (u')	216.9	25.0	10.4	7.4	4.6	2.5	6318/6400

Table 2. RMS of the mean of the distributions of the relative shift between overlapping module pairs, scaled by $1/\sqrt{2}$ to account for the two independent measurements. Results are shown for the three data and two MC geometries described in the text.

	before [μm]	survey [μm]	combined [μm]	combined MC [μm]	ideal MC [μm]
BPIX (u)	114	121	5.7	4.3	4.4
BPIX (v)	122	110	12.7	4.7	4.2
TIB (u)	264	187	7.0	1.6	1.1
TOB (u)	118	118	5.1	2.1	1.6

the reconstructed hits and the predicted positions allow an assessment of the relative alignment between two adjacent modules. A non-zero mean of a Gaussian fit to the distribution of residual differences indicates a relative shift between the modules. A relative rotation between the modules can be seen in the dependence of the differences between the residuals and the track position predictions on the modules under study, where the slope indicates the magnitude of the residual rotation. This would also lead to an increase in the width of the Gaussian fitted to the distribution of the differences between the residuals, and can be minimized by requiring that the slopes be small, as is done in the hit resolution measurement [7]. Any quantitative assessment is nevertheless difficult since it is not easy to disentangle the contributions of the rotations around the different axes.

Only events with a single reconstructed track were used in this analysis. Module pairs with more than 35 (100) hits in the overlap region were analyzed in the pixel (strip) detectors. Only barrel layers satisfied these requirements. The lower hit requirement in the pixel modules reflects their smaller area and leads to correspondingly less precise mean values.

2010 JINST 5 T03009

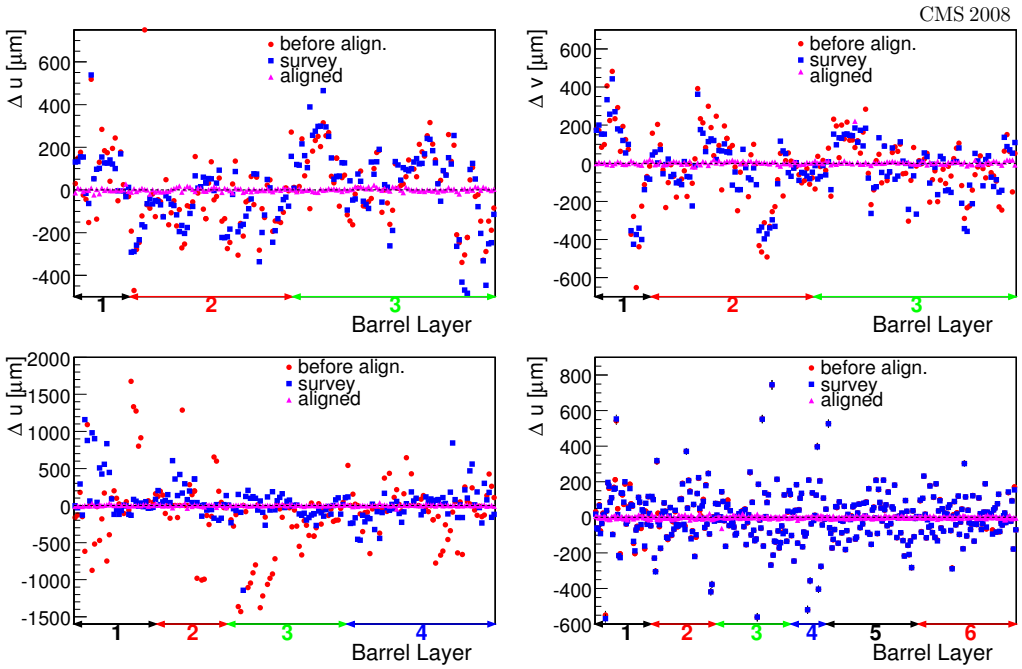

Figure 8. Relative shift between module pairs in the local u (top left) and local v (top right) direction in the BPIX, in the local u-coordinate in the TIB (bottom left), and TOB (bottom right). Only modules in the slice $80^\circ < \phi < 100^\circ$ are shown in the TIB and TOB.

The relative shifts are shown in figure 8. In the strip detectors, the relative shift can be measured in the local u-coordinate. In the pixel detector, this shift can be measured both in the local u and local v coordinates. The RMS of the distribution of the mean values are given in table 2, where the values are scaled by $1/\sqrt{2}$ to account for two independent measurements. The corresponding mean values of the distributions after alignment are 1.5 μm or less. The expectation from MC, for both aligned as well as ideal geometry, is in good agreement with the distribution of the median of residuals quoted in table 1, where results in the pixel detector are more affected by the small size of the overlap sample. The differences in data may be a sign of yet unquantified systematic effects, like the aplanar distortions of modules. While the distributions of hit residuals taken over the full active region of the modules tend to be well centered, this is not always the case for distributions in the overlap regions, which are located at the edges of the active areas in the modules. However, this effect is smaller then 10 μm in the most precise u direction and is 13 μm in the v direction in the pixel barrel modules. There is also visible improvement of the results with survey geometry compared to the geometry before alignment in the TIB, while in the TOB no module-level survey was done and in the BPIX no survey data between overlapping ladders were used either.

5.4 Track parameter resolution

The track parameter resolutions can be validated with independent reconstruction of the upper and the lower portions of cosmic ray tracks and comparison of track parameters at the point of closest approach to the nominal beamline. Both the upper and lower track segments were required to have

2010 JINST 5 T03009

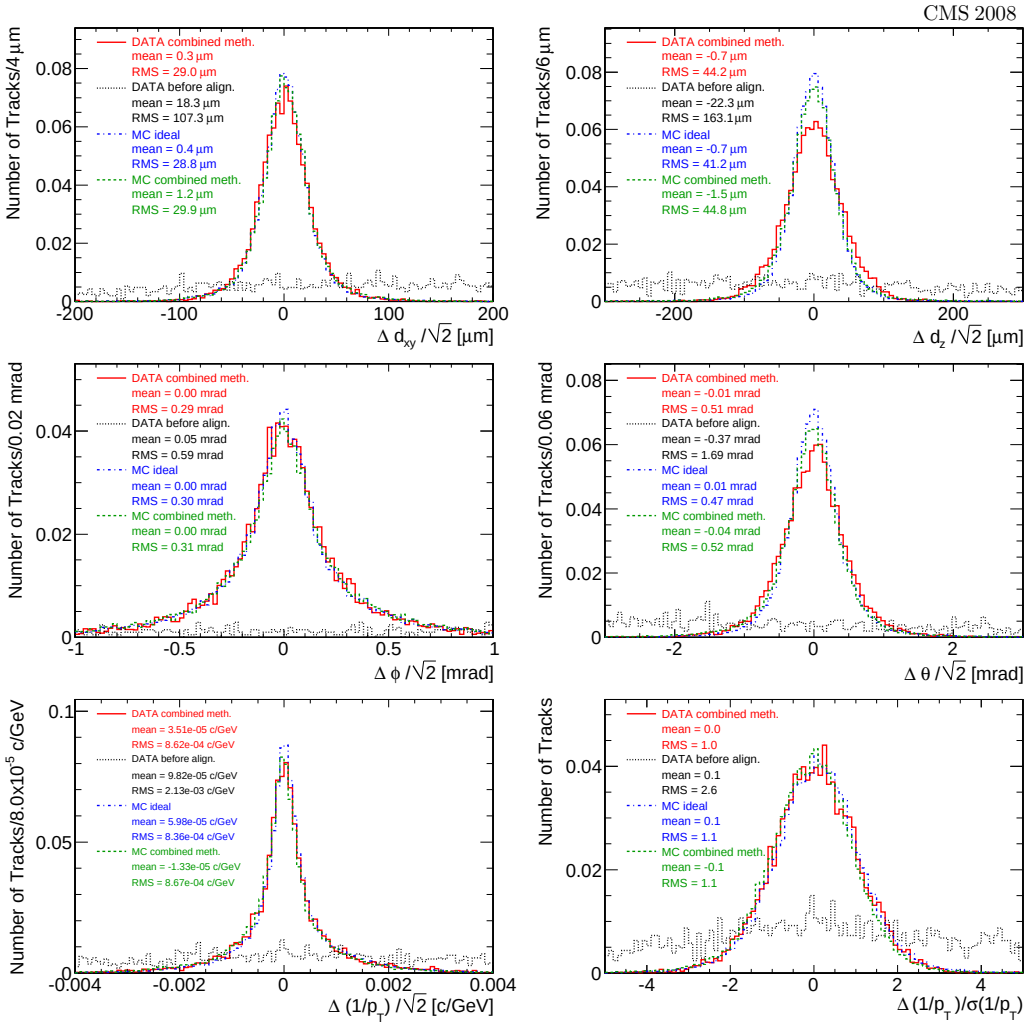

Figure 9. Differences between upper and lower track segment parameters measured at the point of closest approach to the beamline and scaled by $1/\sqrt{2}$. Distributions are shown for the distance of closest approach in the transverse direction d_{xy} (top left), the same in the longitudinal direction d_z (top right), the track azimuthal angle ϕ (middle left), the track polar angle θ (middle right), and $1/p_T$ (bottom left). The plot on the bottom right shows the $1/p_T$ difference normalized to its error, that is $(1/p_{T,1} - 1/p_{T,2})/\sqrt{\sigma^2_{1/p_T,1} + \sigma^2_{1/p_T,2}}$. Results are shown for four geometries: data before alignment (black dotted lines), data with combined method alignment (red solid), combined method MC (green dashed), and ideal MC (blue dash-dotted).

at least three pixel hits. This mimics the topology of collision tracks. The track segments were reconstructed independently. Figure 9 shows the difference between upper and lower portions of tracks for all five track parameters. There is significant improvement due to tracker alignment, with good agreement between data and MC simulations. The results of the combined method are approaching those of a MC simulation with ideal detector geometry. The p_T measurements are most sensitive to the strip part of the tracker, while the other four parameters are dominated by the alignment of the pixel detector. The normalized distributions in figure 9 also show that the error estimates on the track parameters are in good agreement with predictions from MC simulations. Figure 10 shows the dependence of the resolution on p_T for the track parameters d_{xy} and $1/p_T$.

2010 JINST 5 T03009

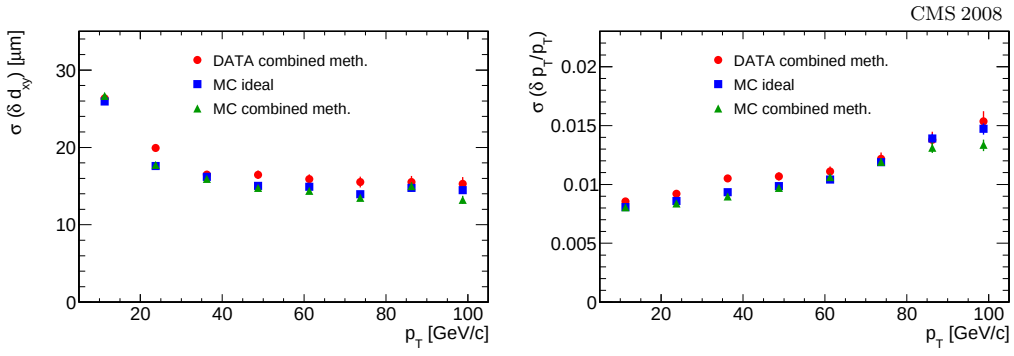

Figure 10. Dependence on p_T of the differences between the track parameters measured at the point of closest approach to the nominal beamline, in the two halves of a cosmic ray track and scaled by $1/\sqrt{2}$. The RMS of the distribution truncated at 95% is quoted at each momentum interval, shown for the distance of closest approach in the transverse direction d_{xy} (left) and for $1/p_T$ (right). Results are shown for the geometries derived from ideal MC (blue squares), and from the alignment result with cosmic ray data (red circles) and combined method MC (green triangles).

5.5 Systematic misalignment studies

A global translation and rotation of the whole tracker is an example of a trivial transformation which leaves the χ^2 value of eq. (4.1) unchanged. This transformation has no effect on the internal alignment and is easily resolved by a suitable convention when defining the global reference frame. The convention that the center-of-gravity of all modules coincides with the design position was used in this work. A similar convention was used for the rotation of the tracker.

There are, however, non-trivial transformations, so-called "weak" modes, that also preserve the χ^2 value of eq. (4.1) and are of larger concern. The presence of weak modes in the geometry resulting from track-based alignment was investigated following the approach described in ref. [15]. Nine systematic distortions, in Δr, $\Delta\phi$, and Δz as a function of r, ϕ, and z were applied to the aligned geometry. Studies were performed with both global and local alignment methods and the results presented here were obtained with the global method. The systematically misaligned geometries were used as a starting point and the alignment procedure described in section 4 was repeated. The nine geometries obtained after the alignments were then compared to the original aligned geometry to see if the distortions can be recovered by the alignment procedure.

The results were analyzed separately for the pixel (BPIX and FPIX), barrel strip (TIB and TOB), and forward strip (TID and TEC) sub-detectors. The remaining displacements of the modules in the TIB and TOB, which are expected to have the best illumination from cosmic ray tracks, are shown in figure 11 for four systematic deformations: the layer rotation ($\Delta\phi = c_1 + c_2 r$), the twist deformation ($\Delta\phi = c_1 z$), the skew ($\Delta z = c_1 \cos\phi$), and the z-expansion ($\Delta z = c_1 z$). The layer rotation can be well recovered in alignment with cosmic ray tracks, while the scatter in the module position difference is an evidence for weak modes in other projections. The twist and the skew deformations are reflected to a lesser degree in track χ^2, and therefore are only partially recovered. Finally, as the distribution of the track χ^2 changes only marginally with respect to the z-expansion, this deformation cannot be recovered using cosmic ray tracks only.

2010 JINST 5 T03009

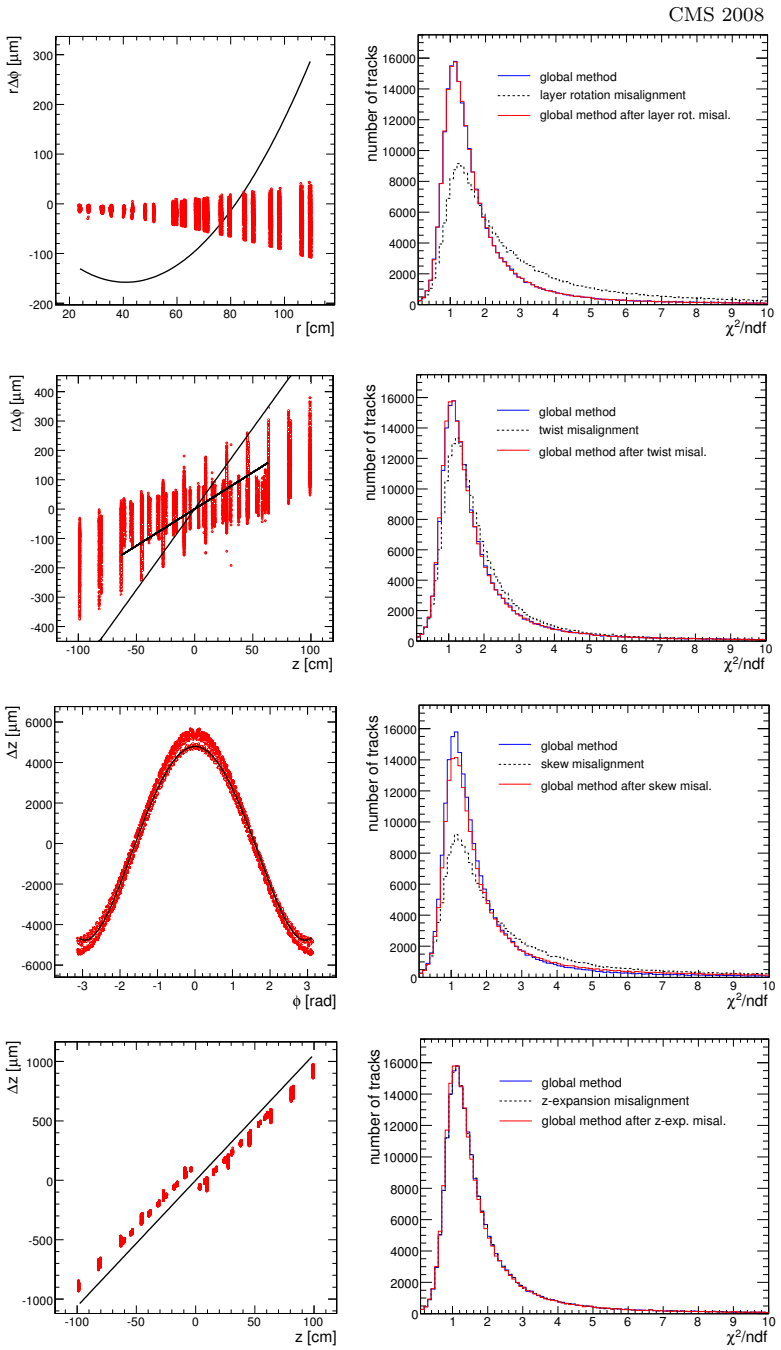

Figure 11. Comparison of the position of the TIB and TOB modules with respect to the geometry obtained with the global method after applying systematic distortions (black solid lines) and after alignment (red dots) is shown on the left for layer rotation (top row), twist (second row), skew (third row), and z-expansion (bottom row) weak modes. For the twist misalignment, the shorter and longer solid lines correspond to the modules in the inner layer of the TIB and in the outer layer of the TOB, respectively. The plots on the right show the distributions of the corresponding track χ^2/ndf after the alignment with the global method (blue solid line), after introducing the systematic misalignment (black dashed line), and after re-aligning (red solid line, below the blue solid line).

2010 JINST 5 T03009

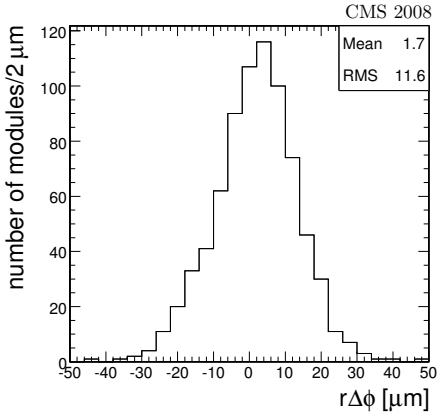

Figure 12. Differences of the BPIX module positions $r(\phi_{\text{local}} - \phi_{\text{global}})$ as obtained with the local and global methods.

Radial deformations are generally recovered using constraints from overlapping modules. Also, mid-plane differences between the upper and lower legs of cosmic ray tracks are sensitive to deformations that differently affect the upper and lower parts of the tracker, including the layer rotation and telescope ($\Delta z = c_1 r$) modes. However, more subtle deformations, including those discussed above, may be difficult to recover with cosmic ray tracks alone. Additional information with tracks from LHC beam interactions, which should be uniform in ϕ, and with additional constraints from the verticies and the masses of resonances, may provide better sensitivity to those systematic deformations. In principle, the Laser Aligment System (section 5.7) and hierarchical survey measurements provide complementary information, but evaluating systematic biases in those measurements is a challenging task.

5.6 Study of detector geometry

Two sets of comparisons between geometries obtained from track-based alignment with data have been performed: a comparison between the geometries from the local and the global methods, and a comparison between the geometry obtained with the combined method with respect to the design one. A comparison between two geometries is done after correcting for an overall residual shift and rotation of the whole detector, or a sub-detector, with respect to its center-of-gravity.

Figure 12 shows the distribution of the differences between the $r\phi$ positions of the 768 BPIX modules obtained with the local and the global methods. The RMS of the distribution is about 12 μm. The distribution of the differences between the z positions is similar once the two main weak modes, Δz vs. z and Δz vs. ϕ, are properly identified and removed by the means of the fit with the functions shown in the left of figure 11. Similar module-by-module comparisons were performed on larger structures, like the TIB or TOB, where weak modes cannot be easily removed, and on coordinates for which the track-based alignment with cosmic rays has a limited sensitivity. This led to distributions characterized by a larger spread. This is also confirmed by alignment on simulated data and limits the accuracy of the absolute position determination.

Assuming that the geometry of the tracker is best described by the one obtained with the

2010 JINST 5 T03009

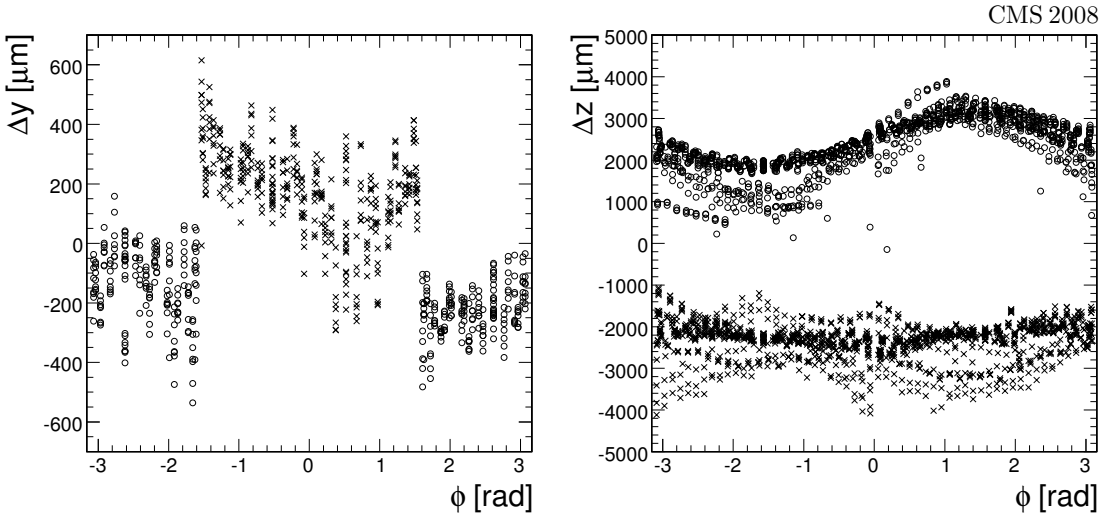

Figure 13. Comparison of the position of the modules in the combined method geometry with respect to the design one: $(y_{design} - y_{comb})$ for the BPIX modules (left) and $(z_{design} - z_{comb})$ for the TIB modules (right) as a function of ϕ. In the plot on the left crosses (circles) represent modules of the positive (negative) x BPIX half-barrel. In the plot on the right crosses (circles) represent modules of the positive (negative) z TIB half-barrel.

combined method, a comparison with the design geometry indicates that the two BPIX half-barrels are shifted along the vertical axis by about 0.4 mm and the two half-barrels of the TIB have an extra separation along the z axis of about 5 mm. Both displacements are mechanically possible. The large displacement of the TIB half-barrels is supported by the optical survey measurements described in ref. [9]. Figure 13 shows the displacement in the y- and in the z-coordinates of the BPIX and TIB modules with respect to the design position. In the case of the TIB, a large scatter of the z-coordinate of the modules with respect to their design position is observed. The modulation of the displacement as a function of the ϕ position of the module can be explained by the presence of the weak mode skew in the combined geometry, as discussed in the previous section.

5.7 Validation with the Laser Alignment System

An independent test of the silicon tracker alignment was provided by the Laser Alignment System (LAS), which uses a system of 40 infrared laser beams ($\lambda = 1075$ nm) to survey the position of the large-scale structure elements of the tracker. The LAS measurements are available for 434 silicon strip modules, which are distributed over eight azimuthal sectors. The light is detected directly on the active area of the silicon sensors and therefore provides excellent beam position resolution with respect to the module sensitive area. For each TEC disk, there are 16 modules distributed uniformly in ϕ at two radial positions that are intersected by laser beams. Furthermore, the LAS is capable of measuring the relative orientation of both endcaps and the TIB and TOB half-barrels. The TID and the pixel detector are not included in the LAS.

Operation of the LAS during data-taking was mainly devoted to commissioning. In total, 31 out of the 40 laser beams were fully operational during this period. The available data were used

2010 JINST 5 T03009

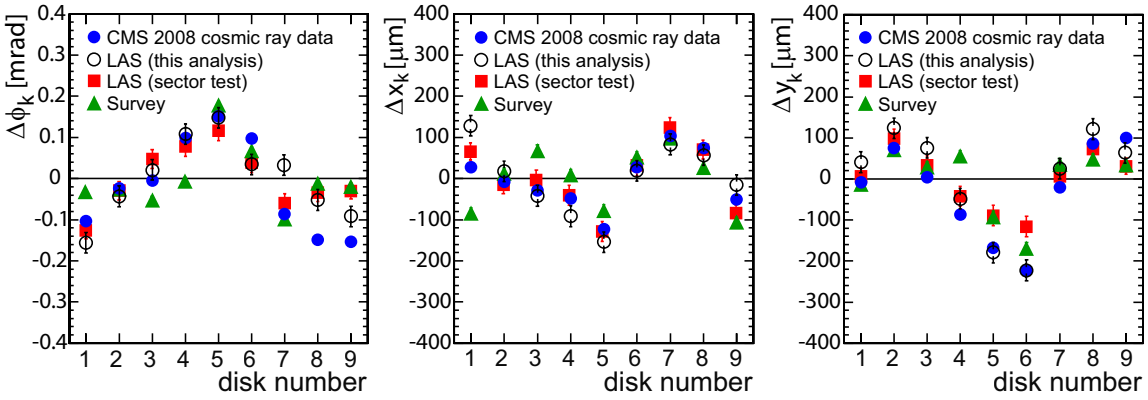

Figure 14. The three alignment parameters for positive z TEC disks measured using cosmic ray data (solid blue circles), by the LAS in this analysis (open black circles), during the LAS sector test [9] (red squares), and by optical survey (green triangles): rotation around global z (left) and translation in global x (middle) and in global y (right).

to calculate the relative positions of the TEC disks. Using LAS measurements in the alignment procedure by means of additional terms to eq. (4.1) is not discussed in this paper.

For the calculation of the alignment parameters from LAS data, the TEC disks were treated as solid objects, each with one rotational and two translational degrees of freedom. Additional degrees of freedom resulted from the fact that the beam directions may deviate from their nominal values at the level of 1 mrad. The calculation was based on an analytical approach for solving the χ^2-minimization problem for the laser hit residuals.

For comparison, the position of the TEC disks was also calculated from the results of the track-based alignment using the combined method, where only the position of the modules illuminated by the LAS beams were considered, for consistency. Figure 14 compares the results of the measurements for positive z side TEC disks from the cosmic ray data analysis, the LAS data analysis, the LAS sector test [9], and optical survey. All data are in good agreement. However, it is difficult to estimate the systematic uncertainties in the results for the track-based alignment due to the effects discussed in section 5.5. Small movements of particular disks are expected between the sector test and optical survey measurements and the CRAFT results from the LAS and the track-based alignment. The optical surveys were done with the endcaps in a vertical orientation whereas they have a horizontal orientation within the tracker.

As a comparison to track-based results, the laser hit residuals, defined as the difference between the nominal and the measured laser hit position along the ϕ-coordinate, have been determined from the tracker geometry before alignment as well as assuming the geometry from the combined method. Corrections have been made for deviations of the beams from their nominal orientations. The results are shown in figure 15. Assuming the aligned geometry as measured with tracks, the overall RMS of the residual distribution decreases significantly with respect to the before alignment case (cf. table 3). For the modules in the TEC, the RMS decreases by more than a factor of two, while the effect in the TOB is slightly smaller. The largest relative improvement is observed for the TIB modules. However, the resulting RMS of 200 μrad for TIB modules remains

2010 JINST 5 T03009

Table 3. RMS of laser hit residuals ($\phi_{\text{nominal}} - \phi_{\text{measured}}$) for the TEC, TIB, and TOB before and after alignment with the combined alignment method.

	TIB [μrad]	TOB [μrad]	TEC [μrad]
before align.	790	200	160
aligned	200	110	70

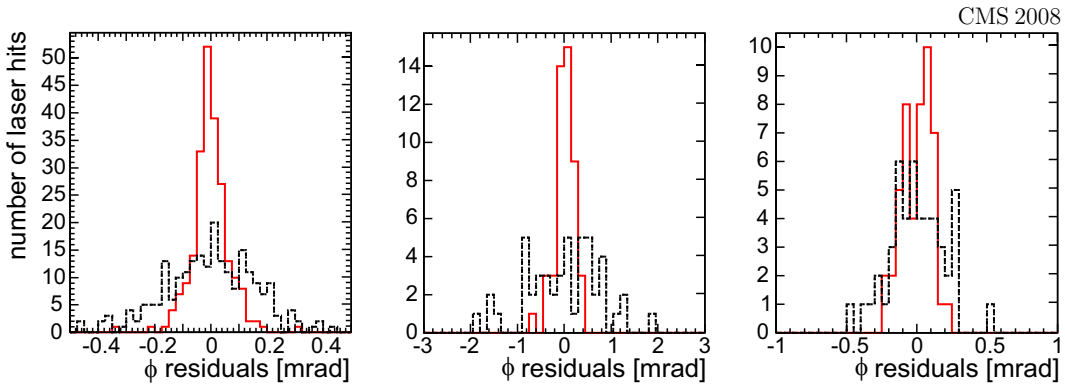

Figure 15. Laser hit residuals ($\phi_{\text{nominal}} - \phi_{\text{measured}}$) for the TEC (left), TIB (middle), and TOB (right), using the geometry before alignment (dashed black line) and the geometry obtained from the combined alignment method (solid red line).

larger than in the other sub-detectors. The observed residual widths may reflect an insufficient calibration of the lasers and a non-optimized laser beam correction procedure. Furthermore, weak modes for which the track-based alignment with cosmic rays has limited sensitivity may contribute to the residual distributions observed in the LAS studies.

6 Summary and discussion

In summary, results of the first full alignment of the CMS tracker have been presented. Two algorithms have been used to determine the positions of all 16 588 silicon modules. The two alignment methods have been combined sequentially to take into account most effectively both global and local correlations of module positions. The results are based on the analysis of about three million cosmic ray tracks recorded with a 3.8 T magnetic field.

The precision of the detector positions with respect to particle trajectories has been derived from the distribution of the median of the cosmic muon track residuals to be on average 3–4 μm RMS in the barrel and 3–14 μm RMS in the endcaps in the most sensitive coordinate. These results are supported by the difference of the residuals in regions where modules overlap within a layer, thus reducing effects of multiple scattering in the calculation of the residuals. Nevertheless, additional small systematic effects may still be present. The achieved tracker resolution in all five track parameters has been checked with a study of the two halves of a cosmic ray track and

2010 JINST 5 T03009

compared with predictions from a detailed detector simulation. The measured resolutions are close to those that would be observed in a detector with perfectly placed modules.

Overall, a significant improvement in track fit performance compared either to using the before alignment or survey geometry has been observed. The resulting aligned geometry allows a study of the assembly precision of the individual sub-detectors. A comparison of module positions obtained with complementary methods supports findings based on track residuals. Nonetheless, certain deformations in the geometry that do not change the χ^2 of the tracks, cannot be ruled out due to the largely vertical nature of the cosmic track data.

Clear improvement in the LAS residuals is observed when using the result of the track based alignment. The stand-alone LAS data analysis agrees well with that from previous tests and with survey alignment. The operation of the LAS has shown that the laser beams operate properly.

Experience gained in the alignment analysis of the silicon modules with cosmic ray particles is valuable in preparation for the CMS tracker alignment with the data from LHC collisions, which is critical to achieving the physics goals of the CMS detector. Integration of measurements from cosmic ray and collision tracks, LAS, and survey will be critical for the optimal tracker alignment with the first data expected from LHC beam collisions. Because the track parameter resolutions are close to the design performance with cosmic ray data already, statistical uncertainties in track parameters are not expected to be considerably affected by alignment at CMS startup with data from beam collisions.

Acknowledgments

We thank the technical and administrative staff at CERN and other CMS Institutes, and acknowledge support from: FMSR (Austria); FNRS and FWO (Belgium); CNPq, CAPES, FAPERJ, and FAPESP (Brazil); MES (Bulgaria); CERN; CAS, MoST, and NSFC (China); COLCIENCIAS (Colombia); MSES (Croatia); RPF (Cyprus); Academy of Sciences and NICPB (Estonia); Academy of Finland, ME, and HIP (Finland); CEA and CNRS/IN2P3 (France); BMBF, DFG, and HGF (Germany); GSRT (Greece); OTKA and NKTH (Hungary); DAE and DST (India); IPM (Iran); SFI (Ireland); INFN (Italy); NRF (Korea); LAS (Lithuania); CINVESTAV, CONACYT, SEP, and UASLP-FAI (Mexico); PAEC (Pakistan); SCSR (Poland); FCT (Portugal); JINR (Armenia, Belarus, Georgia, Ukraine, Uzbekistan); MST and MAE (Russia); MSTDS (Serbia); MICINN and CPAN (Spain); Swiss Funding Agencies (Switzerland); NSC (Taipei); TUBITAK and TAEK (Turkey); STFC (United Kingdom); DOE and NSF (USA). Individuals have received support from the Marie-Curie IEF program (European Union); the Leventis Foundation; the A. P. Sloan Foundation; and the Alexander von Humboldt Foundation.

References

[1] CMS collaboration, *The CMS experiment at the CERN LHC*, 2008 *JINST* **3** S08004.

[2] L. Evans and P. Bryant eds., *LHC Machine*, 2008 *JINST* **3** S08001.

[3] CMS collaboration, *The CMS tracker system project: technical design report*, CERN-LHCC-98-006 (1998).

2010 JINST 5 T03009

[4] CMS collaboration, *The CMS tracker: addendum to the technical design report*, CERN-LHCC-2000-016, CMS-TDR-005-add-1 (2000).

[5] CMS collaboration, *The CMS physics: technical design report, volume 1*, CERN-LHCC-2006-001 (2006).

[6] CMS collaboration, *Commissioning of the CMS experiment and the cosmic run at four tesla*, 2010 *JINST* **4** T03001.

[7] CMS collaboration, *Commissioning and performance of the CMS silicon strip tracker with cosmic ray muons*, 2010 *JINST* **4** T03008.

[8] CMS collaboration, *Commissioning and performance of the CMS pixel tracker with cosmic ray muons*, 2010 *JINST* **4** T03007.

[9] CMS Tracker collaboration, *Alignment of the CMS silicon strip tracker during stand-alone commissioning*, 2009 *JINST* **4** T07001 [arXiv:0904.1220].

[10] P.A. Biallass, T. Hebbeker and K. Hoepfner, *Simulation of cosmic muons and comparison with data from the Cosmic Challenge using drift tube chambers*, CMS-NOTE-2007-024 (2007).

[11] M. Swartz et al., *A new technique for the reconstruction, validation, and simulation of hits in the CMS pixel detector*, CMS-NOTE-2007-033 (2007).

[12] V. Blobel, *Software alignment for tracking detectors*, *Nucl. Instrum. Meth.* **A 566** (2006) 5.

[13] G. Flucke, P. Schleper, G. Steinbrück and M. Stoye, *CMS silicon tracker alignment strategy with the Millepede II algorithm*, 2008 *JINST* **3** P09002.

[14] V. Karimäki, T. Lampén and F.P. Schilling, *The HIP algorithm for track based alignment and its application to the CMS pixel detector*, CMS-NOTE-2006-018 (2006).

[15] D.N. Brown, A.V. Gritsan, Z.J. Guo and D. Roberts, *Local alignment of the BABAR silicon vertex tracker*, *Nucl. Instrum. Meth.* **A 603** (2009) 467.

[16] CMS Tracker collaboration, *Stand-alone cosmic muon reconstruction before installation of the CMS silicon strip tracker*, 2009 *JINST* **4** P05004.

2010 JINST 5 T03009

The CMS collaboration

Yerevan Physics Institute, Yerevan, Armenia
S. Chatrchyan, V. Khachatryan, A.M. Sirunyan

Institut für Hochenergiephysik der OeAW, Wien, Austria
W. Adam, B. Arnold, H. Bergauer, T. Bergauer, M. Dragicevic, M. Eichberger, J. Erö, M. Friedl, R. Frühwirth, V.M. Ghete, J. Hammer[1], S. Hänsel, M. Hoch, N. Hörmann, J. Hrubec, M. Jeitler, G. Kasieczka, K. Kastner, M. Krammer, D. Liko, I. Magrans de Abril, I. Mikulec, F. Mittermayr, B. Neuherz, M. Oberegger, M. Padrta, M. Pernicka, H. Rohringer, S. Schmid, R. Schöfbeck, T. Schreiner, R. Stark, H. Steininger, J. Strauss, A. Taurok, F. Teischinger, T. Themel, D. Uhl, P. Wagner, W. Waltenberger, G. Walzel, E. Widl, C.-E. Wulz

National Centre for Particle and High Energy Physics, Minsk, Belarus
V. Chekhovsky, O. Dvornikov, I. Emeliantchik, A. Litomin, V. Makarenko, I. Marfin, V. Mossolov, N. Shumeiko, A. Solin, R. Stefanovitch, J. Suarez Gonzalez, A. Tikhonov

Research Institute for Nuclear Problems, Minsk, Belarus
A. Fedorov, A. Karneyeu, M. Korzhik, V. Panov, R. Zuyeuski

Research Institute of Applied Physical Problems, Minsk, Belarus
P. Kuchinsky

Universiteit Antwerpen, Antwerpen, Belgium
W. Beaumont, L. Benucci, M. Cardaci, E.A. De Wolf, E. Delmeire, D. Druzhkin, M. Hashemi, X. Janssen, T. Maes, L. Mucibello, S. Ochesanu, R. Rougny, M. Selvaggi, H. Van Haevermaet, P. Van Mechelen, N. Van Remortel

Vrije Universiteit Brussel, Brussel, Belgium
V. Adler, S. Beauceron, S. Blyweert, J. D'Hondt, S. De Weirdt, O. Devroede, J. Heyninck, A. Kalogeropoulos, J. Maes, M. Maes, M.U. Mozer, S. Tavernier, W. Van Doninck[1], P. Van Mulders, I. Villella

Université Libre de Bruxelles, Bruxelles, Belgium
O. Bouhali, E.C. Chabert, O. Charaf, B. Clerbaux, G. De Lentdecker, V. Dero, S. Elgammal, A.P.R. Gay, G.H. Hammad, P.E. Marage, S. Rugovac, C. Vander Velde, P. Vanlaer, J. Wickens

Ghent University, Ghent, Belgium
M. Grunewald, B. Klein, A. Marinov, D. Ryckbosch, F. Thyssen, M. Tytgat, L. Vanelderen, P. Verwilligen

Université Catholique de Louvain, Louvain-la-Neuve, Belgium
S. Basegmez, G. Bruno, J. Caudron, C. Delaere, P. Demin, D. Favart, A. Giammanco, G. Grégoire, V. Lemaitre, O. Militaru, S. Ovyn, K. Piotrzkowski[1], L. Quertenmont, N. Schul

Université de Mons, Mons, Belgium
N. Beliy, E. Daubie

Centro Brasileiro de Pesquisas Fisicas, Rio de Janeiro, Brazil
G.A. Alves, M.E. Pol, M.H.G. Souza

2010 JINST 5 T03009

Universidade do Estado do Rio de Janeiro, Rio de Janeiro, Brazil
W. Carvalho, D. De Jesus Damiao, C. De Oliveira Martins, S. Fonseca De Souza, L. Mundim, V. Oguri, A. Santoro, S.M. Silva Do Amaral, A. Sznajder

Instituto de Fisica Teorica, Universidade Estadual Paulista, Sao Paulo, Brazil
T.R. Fernandez Perez Tomei, M.A. Ferreira Dias, E. M. Gregores[2], S.F. Novaes

Institute for Nuclear Research and Nuclear Energy, Sofia, Bulgaria
K. Abadjiev[1], T. Anguelov, J. Damgov, N. Darmenov[1], L. Dimitrov, V. Genchev[1], P. Iaydjiev, S. Piperov, S. Stoykova, G. Sultanov, R. Trayanov, I. Vankov

University of Sofia, Sofia, Bulgaria
A. Dimitrov, M. Dyulendarova, V. Kozhuharov, L. Litov, E. Marinova, M. Mateev, B. Pavlov, P. Petkov, Z. Toteva[1]

Institute of High Energy Physics, Beijing, China
G.M. Chen, H.S. Chen, W. Guan, C.H. Jiang, D. Liang, B. Liu, X. Meng, J. Tao, J. Wang, Z. Wang, Z. Xue, Z. Zhang

State Key Lab. of Nucl. Phys. and Tech., Peking University, Beijing, China
Y. Ban, J. Cai, Y. Ge, S. Guo, Z. Hu, Y. Mao, S.J. Qian, H. Teng, B. Zhu

Universidad de Los Andes, Bogota, Colombia
C. Avila, M. Baquero Ruiz, C.A. Carrillo Montoya, A. Gomez, B. Gomez Moreno, A.A. Ocampo Rios, A.F. Osorio Oliveros, D. Reyes Romero, J.C. Sanabria

Technical University of Split, Split, Croatia
N. Godinovic, K. Lelas, R. Plestina, D. Polic, I. Puljak

University of Split, Split, Croatia
Z. Antunovic, M. Dzelalija

Institute Rudjer Boskovic, Zagreb, Croatia
V. Brigljevic, S. Duric, K. Kadija, S. Morovic

University of Cyprus, Nicosia, Cyprus
R. Fereos, M. Galanti, J. Mousa, A. Papadakis, F. Ptochos, P.A. Razis, D. Tsiakkouri, Z. Zinonos

National Institute of Chemical Physics and Biophysics, Tallinn, Estonia
A. Hektor, M. Kadastik, K. Kannike, M. Müntel, M. Raidal, L. Rebane

Helsinki Institute of Physics, Helsinki, Finland
E. Anttila, S. Czellar, J. Härkönen, A. Heikkinen, V. Karimäki, R. Kinnunen, J. Klem, M.J. Kortelainen, T. Lampén, K. Lassila-Perini, S. Lehti, T. Lindén, P. Luukka, T. Mäenpää, J. Nysten, E. Tuominen, J. Tuominiemi, D. Ungaro, L. Wendland

Lappeenranta University of Technology, Lappeenranta, Finland
K. Banzuzi, A. Korpela, T. Tuuva

Laboratoire d'Annecy-le-Vieux de Physique des Particules, IN2P3-CNRS, Annecy-le-Vieux, France
P. Nedelec, D. Sillou

2010 JINST 5 T03009

DSM/IRFU, CEA/Saclay, Gif-sur-Yvette, France
M. Besancon, R. Chipaux, M. Dejardin, D. Denegri, J. Descamps, B. Fabbro, J.L. Faure, F. Ferri, S. Ganjour, F.X. Gentit, A. Givernaud, P. Gras, G. Hamel de Monchenault, P. Jarry, M.C. Lemaire, E. Locci, J. Malcles, M. Marionneau, L. Millischer, J. Rander, A. Rosowsky, D. Rousseau, M. Titov, P. Verrecchia

Laboratoire Leprince-Ringuet, Ecole Polytechnique, IN2P3-CNRS, Palaiseau, France
S. Baffioni, L. Bianchini, M. Bluj[3], P. Busson, C. Charlot, L. Dobrzynski, R. Granier de Cassagnac, M. Haguenauer, P. Miné, P. Paganini, Y. Sirois, C. Thiebaux, A. Zabi

Institut Pluridisciplinaire Hubert Curien, Université de Strasbourg, Université de Haute Alsace Mulhouse, CNRS/IN2P3, Strasbourg, France
J.-L. Agram[4], A. Besson, D. Bloch, D. Bodin, J.-M. Brom, E. Conte[4], F. Drouhin[4], J.-C. Fontaine[4], D. Gelé, U. Goerlach, L. Gross, P. Juillot, A.-C. Le Bihan, Y. Patois, J. Speck, P. Van Hove

Université de Lyon, Université Claude Bernard Lyon 1, CNRS-IN2P3, Institut de Physique Nucléaire de Lyon, Villeurbanne, France
C. Baty, M. Bedjidian, J. Blaha, G. Boudoul, H. Brun, N. Chanon, R. Chierici, D. Contardo, P. Depasse, T. Dupasquier, H. El Mamouni, F. Fassi[5], J. Fay, S. Gascon, B. Ille, T. Kurca, T. Le Grand, M. Lethuillier, N. Lumb, L. Mirabito, S. Perries, M. Vander Donckt, P. Verdier

E. Andronikashvili Institute of Physics, Academy of Science, Tbilisi, Georgia
N. Djaoshvili, N. Roinishvili, V. Roinishvili

Institute of High Energy Physics and Informatization, Tbilisi State University, Tbilisi, Georgia
N. Amaglobeli

RWTH Aachen University, I. Physikalisches Institut, Aachen, Germany
R. Adolphi, G. Anagnostou, R. Brauer, W. Braunschweig, M. Edelhoff, H. Esser, L. Feld, W. Karpinski, A. Khomich, K. Klein, N. Mohr, A. Ostaptchouk, D. Pandoulas, G. Pierschel, F. Raupach, S. Schael, A. Schultz von Dratzig, G. Schwering, D. Sprenger, M. Thomas, M. Weber, B. Wittmer, M. Wlochal

RWTH Aachen University, III. Physikalisches Institut A, Aachen, Germany
O. Actis, G. Altenhöfer, W. Bender, P. Biallass, M. Erdmann, G. Fetchenhauer[1], J. Frangenheim, T. Hebbeker, G. Hilgers, A. Hinzmann, K. Hoepfner, C. Hof, M. Kirsch, T. Klimkovich, P. Kreuzer[1], D. Lanske[†], M. Merschmeyer, A. Meyer, B. Philipps, H. Pieta, H. Reithler, S.A. Schmitz, L. Sonnenschein, M. Sowa, J. Steggemann, H. Szczesny, D. Teyssier, C. Zeidler

RWTH Aachen University, III. Physikalisches Institut B, Aachen, Germany
M. Bontenackels, M. Davids, M. Duda, G. Flügge, H. Geenen, M. Giffels, W. Haj Ahmad, T. Hermanns, D. Heydhausen, S. Kalinin, T. Kress, A. Linn, A. Nowack, L. Perchalla, M. Poettgens, O. Pooth, P. Sauerland, A. Stahl, D. Tornier, M.H. Zoeller

Deutsches Elektronen-Synchrotron, Hamburg, Germany
M. Aldaya Martin, U. Behrens, K. Borras, A. Campbell, E. Castro, D. Dammann, G. Eckerlin, A. Flossdorf, G. Flucke, A. Geiser, D. Hatton, J. Hauk, H. Jung, M. Kasemann, I. Katkov, C. Kleinwort, H. Kluge, A. Knutsson, E. Kuznetsova, W. Lange, W. Lohmann, R. Mankel[1], M. Marienfeld,

2010 JINST 5 T03009

A.B. Meyer, S. Miglioranzi, J. Mnich, M. Ohlerich, J. Olzem, A. Parenti, C. Rosemann, R. Schmidt, T. Schoerner-Sadenius, D. Volyanskyy, C. Wissing, W.D. Zeuner[1]

University of Hamburg, Hamburg, Germany
C. Autermann, F. Bechtel, J. Draeger, D. Eckstein, U. Gebbert, K. Kaschube, G. Kaussen, R. Klanner, B. Mura, S. Naumann-Emme, F. Nowak, U. Pein, C. Sander, P. Schleper, T. Schum, H. Stadie, G. Steinbrück, J. Thomsen, R. Wolf

Institut für Experimentelle Kernphysik, Karlsruhe, Germany
J. Bauer, P. Blüm, V. Buege, A. Cakir, T. Chwalek, W. De Boer, A. Dierlamm, G. Dirkes, M. Feindt, U. Felzmann, M. Frey, A. Furgeri, J. Gruschke, C. Hackstein, F. Hartmann[1], S. Heier, M. Heinrich, H. Held, D. Hirschbuehl, K.H. Hoffmann, S. Honc, C. Jung, T. Kuhr, T. Liamsuwan, D. Martschei, S. Mueller, Th. Müller, M.B. Neuland, M. Niegel, O. Oberst, A. Oehler, J. Ott, T. Peiffer, D. Piparo, G. Quast, K. Rabbertz, F. Ratnikov, N. Ratnikova, M. Renz, C. Saout[1], G. Sartisohn, A. Scheurer, P. Schieferdecker, F.-P. Schilling, G. Schott, H.J. Simonis, F.M. Stober, P. Sturm, D. Troendle, A. Trunov, W. Wagner, J. Wagner-Kuhr, M. Zeise, V. Zhukov[6], E.B. Ziebarth

Institute of Nuclear Physics "Demokritos", Aghia Paraskevi, Greece
G. Daskalakis, T. Geralis, K. Karafasoulis, A. Kyriakis, D. Loukas, A. Markou, C. Markou, C. Mavrommatis, E. Petrakou, A. Zachariadou

University of Athens, Athens, Greece
L. Gouskos, P. Katsas, A. Panagiotou[1]

University of Ioánnina, Ioánnina, Greece
I. Evangelou, P. Kokkas, N. Manthos, I. Papadopoulos, V. Patras, F.A. Triantis

KFKI Research Institute for Particle and Nuclear Physics, Budapest, Hungary
G. Bencze[1], L. Boldizsar, G. Debreczeni, C. Hajdu[1], S. Hernath, P. Hidas, D. Horvath[7], K. Krajczar, A. Laszlo, G. Patay, F. Sikler, N. Toth, G. Vesztergombi

Institute of Nuclear Research ATOMKI, Debrecen, Hungary
N. Beni, G. Christian, J. Imrek, J. Molnar, D. Novak, J. Palinkas, G. Szekely, Z. Szillasi[1], K. Tokesi, V. Veszpremi

University of Debrecen, Debrecen, Hungary
A. Kapusi, G. Marian, P. Raics, Z. Szabo, Z.L. Trocsanyi, B. Ujvari, G. Zilizi

Panjab University, Chandigarh, India
S. Bansal, H.S. Bawa, S.B. Beri, V. Bhatnagar, M. Jindal, M. Kaur, R. Kaur, J.M. Kohli, M.Z. Mehta, N. Nishu, L.K. Saini, A. Sharma, A. Singh, J.B. Singh, S.P. Singh

University of Delhi, Delhi, India
S. Ahuja, S. Arora, S. Bhattacharya[8], S. Chauhan, B.C. Choudhary, P. Gupta, S. Jain, S. Jain, M. Jha, A. Kumar, K. Ranjan, R.K. Shivpuri, A.K. Srivastava

Bhabha Atomic Research Centre, Mumbai, India
R.K. Choudhury, D. Dutta, S. Kailas, S.K. Kataria, A.K. Mohanty, L.M. Pant, P. Shukla, A. Topkar

Tata Institute of Fundamental Research - EHEP, Mumbai, India
T. Aziz, M. Guchait[9], A. Gurtu, M. Maity[10], D. Majumder, G. Majumder, K. Mazumdar, A. Nayak, A. Saha, K. Sudhakar

2010 JINST 5 T03009

Tata Institute of Fundamental Research - HECR, Mumbai, India
S. Banerjee, S. Dugad, N.K. Mondal

Institute for Studies in Theoretical Physics & Mathematics (IPM), Tehran, Iran
H. Arfaei, H. Bakhshiansohi, A. Fahim, A. Jafari, M. Mohammadi Najafabadi, A. Moshaii, S. Paktinat Mehdiabadi, S. Rouhani, B. Safarzadeh, M. Zeinali

University College Dublin, Dublin, Ireland
M. Felcini

INFN Sezione di Bari [a], Università di Bari [b], Politecnico di Bari [c], Bari, Italy
M. Abbrescia[a,b], L. Barbone[a], F. Chiumarulo[a], A. Clemente[a], A. Colaleo[a], D. Creanza[a,c], G. Cuscela[a], N. De Filippis[a], M. De Palma[a,b], G. De Robertis[a], G. Donvito[a], F. Fedele[a], L. Fiore[a], M. Franco[a], G. Iaselli[a,c], N. Lacalamita[a], F. Loddo[a], L. Lusito[a,b], G. Maggi[a,c], M. Maggi[a], N. Manna[a,b], B. Marangelli[a,b], S. My[a,c], S. Natali[a,b], S. Nuzzo[a,b], G. Papagni[a], S. Piccolomo[a], G.A. Pierro[a], C. Pinto[a], A. Pompili[a,b], G. Pugliese[a,c], R. Rajan[a], A. Ranieri[a], F. Romano[a,c], G. Roselli[a,b], G. Selvaggi[a,b], Y. Shinde[a], L. Silvestris[a], S. Tupputi[a,b], G. Zito[a]

INFN Sezione di Bologna [a], Universita di Bologna [b], Bologna, Italy
G. Abbiendi[a], W. Bacchi[a,b], A.C. Benvenuti[a], M. Boldini[a], D. Bonacorsi[a], S. Braibant-Giacomelli[a,b], V.D. Cafaro[a], S.S. Caiazza[a], P. Capiluppi[a,b], A. Castro[a,b], F.R. Cavallo[a], G. Codispoti[a,b], M. Cuffiani[a,b], I. D'Antone[a], G.M. Dallavalle[a,1], F. Fabbri[a], A. Fanfani[a,b], D. Fasanella[a], P. Giacomelli[a], V. Giordano[a], M. Giunta[a,1], C. Grandi[a], M. Guerzoni[a], S. Marcellini[a], G. Masetti[a,b], A. Montanari[a], F.L. Navarria[a,b], F. Odorici[a], G. Pellegrini[a], A. Perrotta[a], A.M. Rossi[a,b], T. Rovelli[a,b], G. Siroli[a,b], G. Torromeo[a], R. Travaglini[a,b]

INFN Sezione di Catania [a], Universita di Catania [b], Catania, Italy
S. Albergo[a,b], S. Costa[a,b], R. Potenza[a,b], A. Tricomi[a,b], C. Tuve[a]

INFN Sezione di Firenze [a], Universita di Firenze [b], Firenze, Italy
G. Barbagli[a], G. Broccolo[a,b], V. Ciulli[a,b], C. Civinini[a], R. D'Alessandro[a,b], E. Focardi[a,b], S. Frosali[a,b], E. Gallo[a], C. Genta[a,b], G. Landi[a,b], P. Lenzi[a,b,1], M. Meschini[a], S. Paoletti[a], G. Sguazzoni[a], A. Tropiano[a]

INFN Laboratori Nazionali di Frascati, Frascati, Italy
L. Benussi, M. Bertani, S. Bianco, S. Colafranceschi[11], D. Colonna[11], F. Fabbri, M. Giardoni, L. Passamonti, D. Piccolo, D. Pierluigi, B. Ponzio, A. Russo

INFN Sezione di Genova, Genova, Italy
P. Fabbricatore, R. Musenich

INFN Sezione di Milano-Biccoca [a], Universita di Milano-Bicocca [b], Milano, Italy
A. Benaglia[a], M. Calloni[a], G.B. Cerati[a,b,1], P. D'Angelo[a], F. De Guio[a], F.M. Farina[a], A. Ghezzi[a], P. Govoni[a,b], M. Malberti[a,b,1], S. Malvezzi[a], A. Martelli[a], D. Menasce[a], V. Miccio[a,b], L. Moroni[a], P. Negri[a,b], M. Paganoni[a,b], D. Pedrini[a], A. Pullia[a,b], S. Ragazzi[a,b], N. Redaelli[a], S. Sala[a], R. Salerno[a,b], T. Tabarelli de Fatis[a,b], V. Tancini[a,b], S. Taroni[a,b]

INFN Sezione di Napoli [a], Universita di Napoli "Federico II" [b], Napoli, Italy
S. Buontempo[a], N. Cavallo[a], A. Cimmino[a,b,1], M. De Gruttola[a,b,1], F. Fabozzi[a,12], A.O.M. Iorio[a], L. Lista[a], D. Lomidze[a], P. Noli[a,b], P. Paolucci[a], C. Sciacca[a,b]

2010 JINST 5 T03009

INFN Sezione di Padova [a], Università di Padova [b], Padova, Italy
P. Azzi[a,1], N. Bacchetta[a], L. Barcellan[a], P. Bellan[a,b,1], M. Bellato[a], M. Benettoni[a], M. Biasotto[a,13], D. Bisello[a,b], E. Borsato[a,b], A. Branca[a], R. Carlin[a,b], L. Castellani[a], P. Checchia[a], E. Conti[a], F. Dal Corso[a], M. De Mattia[a,b], T. Dorigo[a], U. Dosselli[a], F. Fanzago[a], F. Gasparini[a,b], U. Gasparini[a,b], P. Giubilato[a,b], F. Gonella[a], A. Gresele[a,14], M. Gulmini[a,13], A. Kaminskiy[a,b], S. Lacaprara[a,13], I. Lazzizzera[a,14], M. Margoni[a,b], G. Maron[a,13], S. Mattiazzo[a,b], M. Mazzucato[a], M. Meneghelli[a], A.T. Meneguzzo[a,b], M. Michelotto[a], F. Montecassiano[a], M. Nespolo[a], M. Passaseo[a], M. Pegoraro[a], L. Perrozzi[a], N. Pozzobon[a,b], P. Ronchese[a,b], F. Simonetto[a,b], N. Toniolo[a], E. Torassa[a], M. Tosi[a,b], A. Triossi[a], S. Vanini[a,b], S. Ventura[a], P. Zotto[a,b], G. Zumerle[a,b]

INFN Sezione di Pavia [a], Universita di Pavia [b], Pavia, Italy
P. Baesso[a,b], U. Berzano[a], S. Bricola[a], M.M. Necchi[a,b], D. Pagano[a,b], S.P. Ratti[a,b], C. Riccardi[a,b], P. Torre[a,b], A. Vicini[a], P. Vitulo[a,b], C. Viviani[a,b]

INFN Sezione di Perugia [a], Universita di Perugia [b], Perugia, Italy
D. Aisa[a], S. Aisa[a], E. Babucci[a], M. Biasini[a,b], G.M. Bilei[a], B. Caponeri[a,b], B. Checcucci[a], N. Dinu[a], L. Fanò[a], L. Farnesini[a], P. Lariccia[a,b], A. Lucaroni[a,b], G. Mantovani[a,b], A. Nappi[a,b], A. Piluso[a], V. Postolache[a], A. Santocchia[a,b], L. Servoli[a], D. Tonoiu[a], A. Vedaee[a], R. Volpe[a,b]

INFN Sezione di Pisa [a], Universita di Pisa [b], Scuola Normale Superiore di Pisa [c], Pisa, Italy
P. Azzurri[a,c], G. Bagliesi[a], J. Bernardini[a,b], L. Berretta[a], T. Boccali[a], A. Bocci[a,c], L. Borrello[a,c], F. Bosi[a], F. Calzolari[a], R. Castaldi[a], R. Dell'Orso[a], F. Fiori[a,b], L. Foà[a,c], S. Gennai[a,c], A. Giassi[a], A. Kraan[a], F. Ligabue[a,c], T. Lomtadze[a], F. Mariani[a], L. Martini[a], M. Massa[a], A. Messineo[a,b], A. Moggi[a], F. Palla[a], F. Palmonari[a], G. Petragnani[a], G. Petrucciani[a,c], F. Raffaelli[a], S. Sarkar[a], G. Segneri[a], A.T. Serban[a], P. Spagnolo[a,1], R. Tenchini[a,1], S. Tolaini[a], G. Tonelli[a,b,1], A. Venturi[a], P.G. Verdini[a]

INFN Sezione di Roma [a], Universita di Roma "La Sapienza" [b], Roma, Italy
S. Baccaro[a,15], L. Barone[a,b], A. Bartoloni[a], F. Cavallari[a,1], I. Dafinei[a], D. Del Re[a,b], E. Di Marco[a,b], M. Diemoz[a], D. Franci[a,b], E. Longo[a,b], G. Organtini[a,b], A. Palma[a,b], F. Pandolfi[a,b], R. Paramatti[a,1], F. Pellegrino[a], S. Rahatlou[a,b], C. Rovelli[a]

INFN Sezione di Torino [a], Università di Torino [b], Università del Piemonte Orientale (Novara) [c], Torino, Italy
G. Alampi[a], N. Amapane[a,b], R. Arcidiacono[a,b], S. Argiro[a,b], M. Arneodo[a,c], C. Biino[a], M.A. Borgia[a,b], C. Botta[a,b], N. Cartiglia[a], R. Castello[a,b], G. Cerminara[a,b], M. Costa[a,b], D. Dattola[a], G. Dellacasa[a], N. Demaria[a], G. Dughera[a], F. Dumitrache[a], A. Graziano[a,b], C. Mariotti[a], M. Marone[a,b], S. Maselli[a], E. Migliore[a,b], G. Mila[a,b], V. Monaco[a,b], M. Musich[a,b], M. Nervo[a,b], M.M. Obertino[a,c], S. Oggero[a,b], R. Panero[a], N. Pastrone[a], M. Pelliccioni[a,b], A. Romero[a,b], M. Ruspa[a,c], R. Sacchi[a,b], A. Solano[a,b], A. Staiano[a], P.P. Trapani[a,b,1], D. Trocino[a,b], A. Vilela Pereira[a,b], L. Visca[a,b], A. Zampieri[a]

INFN Sezione di Trieste [a], Universita di Trieste [b], Trieste, Italy
F. Ambroglini[a,b], S. Belforte[a], F. Cossutti[a], G. Della Ricca[a,b], B. Gobbo[a], A. Penzo[a]

Kyungpook National University, Daegu, Korea
S. Chang, J. Chung, D.H. Kim, G.N. Kim, D.J. Kong, H. Park, D.C. Son

2010 JINST 5 T03009

Wonkwang University, Iksan, Korea
S.Y. Bahk

Chonnam National University, Kwangju, Korea
S. Song

Konkuk University, Seoul, Korea
S.Y. Jung

Korea University, Seoul, Korea
B. Hong, H. Kim, J.H. Kim, K.S. Lee, D.H. Moon, S.K. Park, H.B. Rhee, K.S. Sim

Seoul National University, Seoul, Korea
J. Kim

University of Seoul, Seoul, Korea
M. Choi, G. Hahn, I.C. Park

Sungkyunkwan University, Suwon, Korea
S. Choi, Y. Choi, J. Goh, H. Jeong, T.J. Kim, J. Lee, S. Lee

Vilnius University, Vilnius, Lithuania
M. Janulis, D. Martisiute, P. Petrov, T. Sabonis

Centro de Investigacion y de Estudios Avanzados del IPN, Mexico City, Mexico
H. Castilla Valdez[1], A. Sánchez Hernández

Universidad Iberoamericana, Mexico City, Mexico
S. Carrillo Moreno

Universidad Autónoma de San Luis Potosí, San Luis Potosí, Mexico
A. Morelos Pineda

University of Auckland, Auckland, New Zealand
P. Allfrey, R.N.C. Gray, D. Krofcheck

University of Canterbury, Christchurch, New Zealand
N. Bernardino Rodrigues, P.H. Butler, T. Signal, J.C. Williams

National Centre for Physics, Quaid-I-Azam University, Islamabad, Pakistan
M. Ahmad, I. Ahmed, W. Ahmed, M.I. Asghar, M.I.M. Awan, H.R. Hoorani, I. Hussain, W.A. Khan, T. Khurshid, S. Muhammad, S. Qazi, H. Shahzad

Institute of Experimental Physics, Warsaw, Poland
M. Cwiok, R. Dabrowski, W. Dominik, K. Doroba, M. Konecki, J. Krolikowski, K. Pozniak[16], R. Romaniuk, W. Zabolotny[16], P. Zych

Soltan Institute for Nuclear Studies, Warsaw, Poland
T. Frueboes, R. Gokieli, L. Goscilo, M. Górski, M. Kazana, K. Nawrocki, M. Szleper, G. Wrochna, P. Zalewski

Laboratório de Instrumentação e Física Experimental de Partículas, Lisboa, Portugal
N. Almeida, L. Antunes Pedro, P. Bargassa, A. David, P. Faccioli, P.G. Ferreira Parracho, M. Freitas Ferreira, M. Gallinaro, M. Guerra Jordao, P. Martins, G. Mini, P. Musella, J. Pela, L. Raposo, P.Q. Ribeiro, S. Sampaio, J. Seixas, J. Silva, P. Silva, D. Soares, M. Sousa, J. Varela, H.K. Wöhri

2010 JINST 5 T03009

Joint Institute for Nuclear Research, Dubna, Russia
I. Altsybeev, I. Belotelov, P. Bunin, Y. Ershov, I. Filozova, M. Finger, M. Finger Jr., A. Golunov, I. Golutvin, N. Gorbounov, V. Kalagin, A. Kamenev, V. Karjavin, V. Konoplyanikov, V. Korenkov, G. Kozlov, A. Kurenkov, A. Lanev, A. Makankin, V.V. Mitsyn, P. Moisenz, E. Nikonov, D. Oleynik, V. Palichik, V. Perelygin, A. Petrosyan, R. Semenov, S. Shmatov, V. Smirnov, D. Smolin, E. Tikhonenko, S. Vasil'ev, A. Vishnevskiy, A. Volodko, A. Zarubin, V. Zhiltsov

Petersburg Nuclear Physics Institute, Gatchina (St Petersburg), Russia
N. Bondar, L. Chtchipounov, A. Denisov, Y. Gavrikov, G. Gavrilov, V. Golovtsov, Y. Ivanov, V. Kim, V. Kozlov, P. Levchenko, G. Obrant, E. Orishchin, A. Petrunin, Y. Shcheglov, A. Shchetkovskiy, V. Sknar, I. Smirnov, V. Sulimov, V. Tarakanov, L. Uvarov, S. Vavilov, G. Velichko, S. Volkov, A. Vorobyev

Institute for Nuclear Research, Moscow, Russia
Yu. Andreev, A. Anisimov, P. Antipov, A. Dermenev, S. Gninenko, N. Golubev, M. Kirsanov, N. Krasnikov, V. Matveev, A. Pashenkov, V.E. Postoev, A. Solovey, A. Solovey, A. Toropin, S. Troitsky

Institute for Theoretical and Experimental Physics, Moscow, Russia
A. Baud, V. Epshteyn, V. Gavrilov, N. Ilina, V. Kaftanov†, V. Kolosov, M. Kossov[1], A. Krokhotin, S. Kuleshov, A. Oulianov, G. Safronov, S. Semenov, I. Shreyber, V. Stolin, E. Vlasov, A. Zhokin

Moscow State University, Moscow, Russia
E. Boos, M. Dubinin[17], L. Dudko, A. Ershov, A. Gribushin, V. Klyukhin, O. Kodolova, I. Lokhtin, S. Petrushanko, L. Sarycheva, V. Savrin, A. Snigirev, I. Vardanyan

P.N. Lebedev Physical Institute, Moscow, Russia
I. Dremin, M. Kirakosyan, N. Konovalova, S.V. Rusakov, A. Vinogradov

State Research Center of Russian Federation, Institute for High Energy Physics, Protvino, Russia
S. Akimenko, A. Artamonov, I. Azhgirey, S. Bitioukov, V. Burtovoy, V. Grishin[1], V. Kachanov, D. Konstantinov, V. Krychkine, A. Levine, I. Lobov, V. Lukanin, Y. Mel'nik, V. Petrov, R. Ryutin, S. Slabospitsky, A. Sobol, A. Sytine, L. Tourtchanovitch, S. Troshin, N. Tyurin, A. Uzunian, A. Volkov

Vinca Institute of Nuclear Sciences, Belgrade, Serbia
P. Adzic, M. Djordjevic, D. Jovanovic[18], D. Krpic[18], D. Maletic, J. Puzovic[18], N. Smiljkovic

Centro de Investigaciones Energéticas Medioambientales y Tecnológicas (CIEMAT), Madrid, Spain
M. Aguilar-Benitez, J. Alberdi, J. Alcaraz Maestre, P. Arce, J.M. Barcala, C. Battilana, C. Burgos Lazaro, J. Caballero Bejar, E. Calvo, M. Cardenas Montes, M. Cepeda, M. Cerrada, M. Chamizo Llatas, F. Clemente, N. Colino, M. Daniel, B. De La Cruz, A. Delgado Peris, C. Diez Pardos, C. Fernandez Bedoya, J.P. Fernández Ramos, A. Ferrando, J. Flix, M.C. Fouz, P. Garcia-Abia, A.C. Garcia-Bonilla, O. Gonzalez Lopez, S. Goy Lopez, J.M. Hernandez, M.I. Josa, J. Marin, G. Merino, J. Molina, A. Molinero, J.J. Navarrete, J.C. Oller, J. Puerta Pelayo, L. Romero, J. Santaolalla, C. Villanueva Munoz, C. Willmott, C. Yuste

2010 JINST 5 T03009

Universidad Autónoma de Madrid, Madrid, Spain
C. Albajar, M. Blanco Otano, J.F. de Trocóniz, A. Garcia Raboso, J.O. Lopez Berengueres

Universidad de Oviedo, Oviedo, Spain
J. Cuevas, J. Fernandez Menendez, I. Gonzalez Caballero, L. Lloret Iglesias, H. Naves Sordo, J.M. Vizan Garcia

Instituto de Física de Cantabria (IFCA), CSIC-Universidad de Cantabria, Santander, Spain
I.J. Cabrillo, A. Calderon, S.H. Chuang, I. Diaz Merino, C. Diez Gonzalez, J. Duarte Campderros, M. Fernandez, G. Gomez, J. Gonzalez Sanchez, R. Gonzalez Suarez, C. Jorda, P. Lobelle Pardo, A. Lopez Virto, J. Marco, R. Marco, C. Martinez Rivero, P. Martinez Ruiz del Arbol, F. Matorras, T. Rodrigo, A. Ruiz Jimeno, L. Scodellaro, M. Sobron Sanudo, I. Vila, R. Vilar Cortabitarte

CERN, European Organization for Nuclear Research, Geneva, Switzerland
D. Abbaneo, E. Albert, M. Alidra, S. Ashby, E. Auffray, J. Baechler, P. Baillon, A.H. Ball, S.L. Bally, D. Barney, F. Beaudette[19], R. Bellan, D. Benedetti, G. Benelli, C. Bernet, P. Bloch, S. Bolognesi, M. Bona, J. Bos, N. Bourgeois, T. Bourrel, H. Breuker, K. Bunkowski, D. Campi, T. Camporesi, E. Cano, A. Cattai, J.P. Chatelain, M. Chauvey, T. Christiansen, J.A. Coarasa Perez, A. Conde Garcia, R. Covarelli, B. Curé, A. De Roeck, V. Delachenal, D. Deyrail, S. Di Vincenzo[20], S. Dos Santos, T. Dupont, L.M. Edera, A. Elliott-Peisert, M. Eppard, M. Favre, N. Frank, W. Funk, A. Gaddi, M. Gastal, M. Gateau, H. Gerwig, D. Gigi, K. Gill, D. Giordano, J.P. Girod, F. Glege, R. Gomez-Reino Garrido, R. Goudard, S. Gowdy, R. Guida, L. Guiducci, J. Gutleber, M. Hansen, C. Hartl, J. Harvey, B. Hegner, H.F. Hoffmann, A. Holzner, A. Honma, M. Huhtinen, V. Innocente, P. Janot, G. Le Godec, P. Lecoq, C. Leonidopoulos, R. Loos, C. Lourenço, A. Lyonnet, A. Macpherson, N. Magini, J.D. Maillefaud, G. Maire, T. Mäki, L. Malgeri, M. Mannelli, L. Masetti, F. Meijers, P. Meridiani, S. Mersi, E. Meschi, A. Meynet Cordonnier, R. Moser, M. Mulders, J. Mulon, M. Noy, A. Oh, G. Olesen, A. Onnela, T. Orimoto, L. Orsini, E. Perez, G. Perinic, J.F. Pernot, P. Petagna, P. Petiot, A. Petrilli, A. Pfeiffer, M. Pierini, M. Pimiä, R. Pintus, B. Pirollet, H. Postema, A. Racz, S. Ravat, S.B. Rew, J. Rodrigues Antunes, G. Rolandi[21], M. Rovere, V. Ryjov, H. Sakulin, D. Samyn, H. Sauce, C. Schäfer, W.D. Schlatter, M. Schröder, C. Schwick, A. Sciaba, I. Segoni, A. Sharma, N. Siegrist, P. Siegrist, N. Sinanis, T. Sobrier, P. Sphicas[22], D. Spiga, M. Spiropulu[17], F. Stöckli, P. Traczyk, P. Tropea, J. Troska, A. Tsirou, L. Veillet, G.I. Veres, M. Voutilainen, P. Wertelaers, M. Zanetti

Paul Scherrer Institut, Villigen, Switzerland
W. Bertl, K. Deiters, W. Erdmann, K. Gabathuler, R. Horisberger, Q. Ingram, H.C. Kaestli, S. König, D. Kotlinski, U. Langenegger, F. Meier, D. Renker, T. Rohe, J. Sibille[23], A. Starodumov[24]

Institute for Particle Physics, ETH Zurich, Zurich, Switzerland
B. Betev, L. Caminada[25], Z. Chen, S. Cittolin, D.R. Da Silva Di Calafiori, S. Dambach[25], G. Dissertori, M. Dittmar, C. Eggel[25], J. Eugster, G. Faber, K. Freudenreich, C. Grab, A. Hervé, W. Hintz, P. Lecomte, P.D. Luckey, W. Lustermann, C. Marchica[25], P. Milenovic[26], F. Moortgat, A. Nardulli, F. Nessi-Tedaldi, L. Pape, F. Pauss, T. Punz, A. Rizzi, F.J. Ronga, L. Sala, A.K. Sanchez, M.-C. Sawley, V. Sordini, B. Stieger, L. Tauscher†, A. Thea, K. Theofilatos, D. Treille, P. Trüb[25], M. Weber, L. Wehrli, J. Weng, S. Zelepoukine[27]

2010 JINST 5 T03009

Universität Zürich, Zurich, Switzerland
C. Amsler, V. Chiochia, S. De Visscher, C. Regenfus, P. Robmann, T. Rommerskirchen, A. Schmidt, D. Tsirigkas, L. Wilke

National Central University, Chung-Li, Taiwan
Y.H. Chang, E.A. Chen, W.T. Chen, A. Go, C.M. Kuo, S.W. Li, W. Lin

National Taiwan University (NTU), Taipei, Taiwan
P. Bartalini, P. Chang, Y. Chao, K.F. Chen, W.-S. Hou, Y. Hsiung, Y.J. Lei, S.W. Lin, R.-S. Lu, J. Schümann, J.G. Shiu, Y.M. Tzeng, K. Ueno, Y. Velikzhanin, C.C. Wang, M. Wang

Cukurova University, Adana, Turkey
A. Adiguzel, A. Ayhan, A. Azman Gokce, M.N. Bakirci, S. Cerci, I. Dumanoglu, E. Eskut, S. Girgis, E. Gurpinar, I. Hos, T. Karaman, T. Karaman, A. Kayis Topaksu, P. Kurt, G. Önengüt, G. Önengüt Gökbulut, K. Ozdemir, S. Ozturk, A. Polatöz, K. Sogut[28], B. Tali, H. Topakli, D. Uzun, L.N. Vergili, M. Vergili

Middle East Technical University, Physics Department, Ankara, Turkey
I.V. Akin, T. Aliev, S. Bilmis, M. Deniz, H. Gamsizkan, A.M. Guler, K. Öcalan, M. Serin, R. Sever, U.E. Surat, M. Zeyrek

Bogaziçi University, Department of Physics, Istanbul, Turkey
M. Deliomeroglu, D. Demir[29], E. Gülmez, A. Halu, B. Isildak, M. Kaya[30], O. Kaya[30], S. Ozkorucuklu[31], N. Sonmez[32]

National Scientific Center, Kharkov Institute of Physics and Technology, Kharkov, Ukraine
L. Levchuk, S. Lukyanenko, D. Soroka, S. Zub

University of Bristol, Bristol, United Kingdom
F. Bostock, J.J. Brooke, T.L. Cheng, D. Cussans, R. Frazier, J. Goldstein, N. Grant, M. Hansen, G.P. Heath, H.F. Heath, C. Hill, B. Huckvale, J. Jackson, C.K. Mackay, S. Metson, D.M. Newbold[33], K. Nirunpong, V.J. Smith, J. Velthuis, R. Walton

Rutherford Appleton Laboratory, Didcot, United Kingdom
K.W. Bell, C. Brew, R.M. Brown, B. Camanzi, D.J.A. Cockerill, J.A. Coughlan, N.I. Geddes, K. Harder, S. Harper, B.W. Kennedy, P. Murray, C.H. Shepherd-Themistocleous, I.R. Tomalin, J.H. Williams[†], W.J. Womersley, S.D. Worm

Imperial College, University of London, London, United Kingdom
R. Bainbridge, G. Ball, J. Ballin, R. Beuselinck, O. Buchmuller, D. Colling, N. Cripps, G. Davies, M. Della Negra, C. Foudas, J. Fulcher, D. Futyan, G. Hall, J. Hays, G. Iles, G. Karapostoli, B.C. MacEvoy, A.-M. Magnan, J. Marrouche, J. Nash, A. Nikitenko[24], A. Papageorgiou, M. Pesaresi, K. Petridis, M. Pioppi[34], D.M. Raymond, N. Rompotis, A. Rose, M.J. Ryan, C. Seez, P. Sharp, G. Sidiropoulos[1], M. Stettler, M. Stoye, M. Takahashi, A. Tapper, C. Timlin, S. Tourneur, M. Vazquez Acosta, T. Virdee[1], S. Wakefield, D. Wardrope, T. Whyntie, M. Wingham

Brunel University, Uxbridge, United Kingdom
J.E. Cole, I. Goitom, P.R. Hobson, A. Khan, P. Kyberd, D. Leslie, C. Munro, I.D. Reid, C. Siamitros, R. Taylor, L. Teodorescu, I. Yaselli

2010 JINST 5 T03009

Boston University, Boston, U.S.A.
T. Bose, M. Carleton, E. Hazen, A.H. Heering, A. Heister, J. St. John, P. Lawson, D. Lazic, D. Osborne, J. Rohlf, L. Sulak, S. Wu

Brown University, Providence, U.S.A.
J. Andrea, A. Avetisyan, S. Bhattacharya, J.P. Chou, D. Cutts, S. Esen, G. Kukartsev, G. Landsberg, M. Narain, D. Nguyen, T. Speer, K.V. Tsang

University of California, Davis, Davis, U.S.A.
R. Breedon, M. Calderon De La Barca Sanchez, M. Case, D. Cebra, M. Chertok, J. Conway, P.T. Cox, J. Dolen, R. Erbacher, E. Friis, W. Ko, A. Kopecky, R. Lander, A. Lister, H. Liu, S. Maruyama, T. Miceli, M. Nikolic, D. Pellett, J. Robles, M. Searle, J. Smith, M. Squires, J. Stilley, M. Tripathi, R. Vasquez Sierra, C. Veelken

University of California, Los Angeles, Los Angeles, U.S.A.
V. Andreev, K. Arisaka, D. Cline, R. Cousins, S. Erhan[1], J. Hauser, M. Ignatenko, C. Jarvis, J. Mumford, C. Plager, G. Rakness, P. Schlein[†], J. Tucker, V. Valuev, R. Wallny, X. Yang

University of California, Riverside, Riverside, U.S.A.
J. Babb, M. Bose, A. Chandra, R. Clare, J.A. Ellison, J.W. Gary, G. Hanson, G.Y. Jeng, S.C. Kao, F. Liu, H. Liu, A. Luthra, H. Nguyen, G. Pasztor[35], A. Satpathy, B.C. Shen[†], R. Stringer, J. Sturdy, V. Sytnik, R. Wilken, S. Wimpenny

University of California, San Diego, La Jolla, U.S.A.
J.G. Branson, E. Dusinberre, D. Evans, F. Golf, R. Kelley, M. Lebourgeois, J. Letts, E. Lipeles, B. Mangano, J. Muelmenstaedt, M. Norman, S. Padhi, A. Petrucci, H. Pi, M. Pieri, R. Ranieri, M. Sani, V. Sharma, S. Simon, F. Würthwein, A. Yagil

University of California, Santa Barbara, Santa Barbara, U.S.A.
C. Campagnari, M. D'Alfonso, T. Danielson, J. Garberson, J. Incandela, C. Justus, P. Kalavase, S.A. Koay, D. Kovalskyi, V. Krutelyov, J. Lamb, S. Lowette, V. Pavlunin, F. Rebassoo, J. Ribnik, J. Richman, R. Rossin, D. Stuart, W. To, J.R. Vlimant, M. Witherell

California Institute of Technology, Pasadena, U.S.A.
A. Apresyan, A. Bornheim, J. Bunn, M. Chiorboli, M. Gataullin, D. Kcira, V. Litvine, Y. Ma, H.B. Newman, C. Rogan, V. Timciuc, J. Veverka, R. Wilkinson, Y. Yang, L. Zhang, K. Zhu, R.Y. Zhu

Carnegie Mellon University, Pittsburgh, U.S.A.
B. Akgun, R. Carroll, T. Ferguson, D.W. Jang, S.Y. Jun, M. Paulini, J. Russ, N. Terentyev, H. Vogel, I. Vorobiev

University of Colorado at Boulder, Boulder, U.S.A.
J.P. Cumalat, M.E. Dinardo, B.R. Drell, W.T. Ford, B. Heyburn, E. Luiggi Lopez, U. Nauenberg, K. Stenson, K. Ulmer, S.R. Wagner, S.L. Zang

Cornell University, Ithaca, U.S.A.
L. Agostino, J. Alexander, F. Blekman, D. Cassel, A. Chatterjee, S. Das, L.K. Gibbons, B. Heltsley, W. Hopkins, A. Khukhunaishvili, B. Kreis, V. Kuznetsov, J.R. Patterson, D. Puigh, A. Ryd, X. Shi, S. Stroiney, W. Sun, W.D. Teo, J. Thom, J. Vaughan, Y. Weng, P. Wittich

2010 JINST 5 T03009

Fairfield University, Fairfield, U.S.A.
C.P. Beetz, G. Cirino, C. Sanzeni, D. Winn

Fermi National Accelerator Laboratory, Batavia, U.S.A.
S. Abdullin, M.A. Afaq[1], M. Albrow, B. Ananthan, G. Apollinari, M. Atac, W. Badgett, L. Bagby, J.A. Bakken, B. Baldin, S. Banerjee, K. Banicz, L.A.T. Bauerdick, A. Beretvas, J. Berryhill, P.C. Bhat, K. Biery, M. Binkley, I. Bloch, F. Borcherding, A.M. Brett, K. Burkett, J.N. Butler, V. Chetluru, H.W.K. Cheung, F. Chlebana, I. Churin, S. Cihangir, M. Crawford, W. Dagenhart, M. Demarteau, G. Derylo, D. Dykstra, D.P. Eartly, J.E. Elias, V.D. Elvira, D. Evans, L. Feng, M. Fischler, I. Fisk, S. Foulkes, J. Freeman, P. Gartung, E. Gottschalk, T. Grassi, D. Green, Y. Guo, O. Gutsche, A. Hahn, J. Hanlon, R.M. Harris, B. Holzman, J. Howell, D. Hufnagel, E. James, H. Jensen, M. Johnson, C.D. Jones, U. Joshi, E. Juska, J. Kaiser, B. Klima, S. Kossiakov, K. Kousouris, S. Kwan, C.M. Lei, P. Limon, J.A. Lopez Perez, S. Los, L. Lueking, G. Lukhanin, S. Lusin[1], J. Lykken, K. Maeshima, J.M. Marraffino, D. Mason, P. McBride, T. Miao, K. Mishra, S. Moccia, R. Mommsen, S. Mrenna, A.S. Muhammad, C. Newman-Holmes, C. Noeding, V. O'Dell, O. Prokofyev, R. Rivera, C.H. Rivetta, A. Ronzhin, P. Rossman, S. Ryu, V. Sekhri, E. Sexton-Kennedy, I. Sfiligoi, S. Sharma, T.M. Shaw, D. Shpakov, E. Skup, R.P. Smith[†], A. Soha, W.J. Spalding, L. Spiegel, I. Suzuki, P. Tan, W. Tanenbaum, S. Tkaczyk[1], R. Trentadue[1], L. Uplegger, E.W. Vaandering, R. Vidal, J. Whitmore, E. Wicklund, W. Wu, J. Yarba, F. Yumiceva, J.C. Yun

University of Florida, Gainesville, U.S.A.
D. Acosta, P. Avery, V. Barashko, D. Bourilkov, M. Chen, G.P. Di Giovanni, D. Dobur, A. Drozdetskiy, R.D. Field, Y. Fu, I.K. Furic, J. Gartner, D. Holmes, B. Kim, S. Klimenko, J. Konigsberg, A. Korytov, K. Kotov, A. Kropivnitskaya, T. Kypreos, A. Madorsky, K. Matchev, G. Mitselmakher, Y. Pakhotin, J. Piedra Gomez, C. Prescott, V. Rapsevicius, R. Remington, M. Schmitt, B. Scurlock, D. Wang, J. Yelton

Florida International University, Miami, U.S.A.
C. Ceron, V. Gaultney, L. Kramer, L.M. Lebolo, S. Linn, P. Markowitz, G. Martinez, J.L. Rodriguez

Florida State University, Tallahassee, U.S.A.
T. Adams, A. Askew, H. Baer, M. Bertoldi, J. Chen, W.G.D. Dharmaratna, S.V. Gleyzer, J. Haas, S. Hagopian, V. Hagopian, M. Jenkins, K.F. Johnson, E. Prettner, H. Prosper, S. Sekmen

Florida Institute of Technology, Melbourne, U.S.A.
M.M. Baarmand, S. Guragain, M. Hohlmann, H. Kalakhety, H. Mermerkaya, R. Ralich, I. Vodopiyanov

University of Illinois at Chicago (UIC), Chicago, U.S.A.
B. Abelev, M.R. Adams, I.M. Anghel, L. Apanasevich, V.E. Bazterra, R.R. Betts, J. Callner, M.A. Castro, R. Cavanaugh, C. Dragoiu, E.J. Garcia-Solis, C.E. Gerber, D.J. Hofman, S. Khalatian, C. Mironov, E. Shabalina, A. Smoron, N. Varelas

The University of Iowa, Iowa City, U.S.A.
U. Akgun, E.A. Albayrak, A.S. Ayan, B. Bilki, R. Briggs, K. Cankocak[36], K. Chung, W. Clarida, P. Debbins, F. Duru, F.D. Ingram, C.K. Lae, E. McCliment, J.-P. Merlo, A. Mestvirishvili, M.J. Miller, A. Moeller, J. Nachtman, C.R. Newsom, E. Norbeck, J. Olson, Y. Onel, F. Ozok, J. Parsons, I. Schmidt, S. Sen, J. Wetzel, T. Yetkin, K. Yi

2010 JINST 5 T03009

Johns Hopkins University, Baltimore, U.S.A.
B.A. Barnett, B. Blumenfeld, A. Bonato, C.Y. Chien, D. Fehling, G. Giurgiu, A.V. Gritsan, Z.J. Guo, P. Maksimovic, S. Rappoccio, M. Swartz, N.V. Tran, Y. Zhang

The University of Kansas, Lawrence, U.S.A.
P. Baringer, A. Bean, O. Grachov, M. Murray, V. Radicci, S. Sanders, J.S. Wood, V. Zhukova

Kansas State University, Manhattan, U.S.A.
D. Bandurin, T. Bolton, K. Kaadze, A. Liu, Y. Maravin, D. Onoprienko, I. Svintradze, Z. Wan

Lawrence Livermore National Laboratory, Livermore, U.S.A.
J. Gronberg, J. Hollar, D. Lange, D. Wright

University of Maryland, College Park, U.S.A.
D. Baden, R. Bard, M. Boutemeur, S.C. Eno, D. Ferencek, N.J. Hadley, R.G. Kellogg, M. Kirn, S. Kunori, K. Rossato, P. Rumerio, F. Santanastasio, A. Skuja, J. Temple, M.B. Tonjes, S.C. Tonwar, T. Toole, E. Twedt

Massachusetts Institute of Technology, Cambridge, U.S.A.
B. Alver, G. Bauer, J. Bendavid, W. Busza, E. Butz, I.A. Cali, M. Chan, D. D'Enterria, P. Everaerts, G. Gomez Ceballos, K.A. Hahn, P. Harris, S. Jaditz, Y. Kim, M. Klute, Y.-J. Lee, W. Li, C. Loizides, T. Ma, M. Miller, S. Nahn, C. Paus, C. Roland, G. Roland, M. Rudolph, G. Stephans, K. Sumorok, K. Sung, S. Vaurynovich, E.A. Wenger, B. Wyslouch, S. Xie, Y. Yilmaz, A.S. Yoon

University of Minnesota, Minneapolis, U.S.A.
D. Bailleux, S.I. Cooper, P. Cushman, B. Dahmes, A. De Benedetti, A. Dolgopolov, P.R. Dudero, R. Egeland, G. Franzoni, J. Haupt, A. Inyakin[37], K. Klapoetke, Y. Kubota, J. Mans, N. Mirman, D. Petyt, V. Rekovic, R. Rusack, M. Schroeder, A. Singovsky, J. Zhang

University of Mississippi, University, U.S.A.
L.M. Cremaldi, R. Godang, R. Kroeger, L. Perera, R. Rahmat, D.A. Sanders, P. Sonnek, D. Summers

University of Nebraska-Lincoln, Lincoln, U.S.A.
K. Bloom, B. Bockelman, S. Bose, J. Butt, D.R. Claes, A. Dominguez, M. Eads, J. Keller, T. Kelly, I. Kravchenko, J. Lazo-Flores, C. Lundstedt, H. Malbouisson, S. Malik, G.R. Snow

State University of New York at Buffalo, Buffalo, U.S.A.
U. Baur, I. Iashvili, A. Kharchilava, A. Kumar, K. Smith, M. Strang

Northeastern University, Boston, U.S.A.
G. Alverson, E. Barberis, O. Boeriu, G. Eulisse, G. Govi, T. McCauley, Y. Musienko[38], S. Muzaffar, I. Osborne, T. Paul, S. Reucroft, J. Swain, L. Taylor, L. Tuura

Northwestern University, Evanston, U.S.A.
A. Anastassov, B. Gobbi, A. Kubik, R.A. Ofierzynski, A. Pozdnyakov, M. Schmitt, S. Stoynev, M. Velasco, S. Won

University of Notre Dame, Notre Dame, U.S.A.
L. Antonelli, D. Berry, M. Hildreth, C. Jessop, D.J. Karmgard, T. Kolberg, K. Lannon, S. Lynch, N. Marinelli, D.M. Morse, R. Ruchti, J. Slaunwhite, J. Warchol, M. Wayne

2010 JINST 5 T03009

The Ohio State University, Columbus, U.S.A.
B. Bylsma, L.S. Durkin, J. Gilmore[39], J. Gu, P. Killewald, T.Y. Ling, G. Williams

Princeton University, Princeton, U.S.A.
N. Adam, E. Berry, P. Elmer, A. Garmash, D. Gerbaudo, V. Halyo, A. Hunt, J. Jones, E. Laird, D. Marlow, T. Medvedeva, M. Mooney, J. Olsen, P. Piroué, D. Stickland, C. Tully, J.S. Werner, T. Wildish, Z. Xie, A. Zuranski

University of Puerto Rico, Mayaguez, U.S.A.
J.G. Acosta, M. Bonnett Del Alamo, X.T. Huang, A. Lopez, H. Mendez, S. Oliveros, J.E. Ramirez Vargas, N. Santacruz, A. Zatzerklyany

Purdue University, West Lafayette, U.S.A.
E. Alagoz, E. Antillon, V.E. Barnes, G. Bolla, D. Bortoletto, A. Everett, A.F. Garfinkel, Z. Gecse, L. Gutay, N. Ippolito, M. Jones, O. Koybasi, A.T. Laasanen, N. Leonardo, C. Liu, V. Maroussov, P. Merkel, D.H. Miller, N. Neumeister, A. Sedov, I. Shipsey, H.D. Yoo, Y. Zheng

Purdue University Calumet, Hammond, U.S.A.
P. Jindal, N. Parashar

Rice University, Houston, U.S.A.
V. Cuplov, K.M. Ecklund, F.J.M. Geurts, J.H. Liu, D. Maronde, M. Matveev, B.P. Padley, R. Redjimi, J. Roberts, L. Sabbatini, A. Tumanov

University of Rochester, Rochester, U.S.A.
B. Betchart, A. Bodek, H. Budd, Y.S. Chung, P. de Barbaro, R. Demina, H. Flacher, Y. Gotra, A. Harel, S. Korjenevski, D.C. Miner, D. Orbaker, G. Petrillo, D. Vishnevskiy, M. Zielinski

The Rockefeller University, New York, U.S.A.
A. Bhatti, L. Demortier, K. Goulianos, K. Hatakeyama, G. Lungu, C. Mesropian, M. Yan

Rutgers, the State University of New Jersey, Piscataway, U.S.A.
O. Atramentov, E. Bartz, Y. Gershtein, E. Halkiadakis, D. Hits, A. Lath, K. Rose, S. Schnetzer, S. Somalwar, R. Stone, S. Thomas, T.L. Watts

University of Tennessee, Knoxville, U.S.A.
G. Cerizza, M. Hollingsworth, S. Spanier, Z.C. Yang, A. York

Texas A&M University, College Station, U.S.A.
J. Asaadi, A. Aurisano, R. Eusebi, A. Golyash, A. Gurrola, T. Kamon, C.N. Nguyen, J. Pivarski, A. Safonov, S. Sengupta, D. Toback, M. Weinberger

Texas Tech University, Lubbock, U.S.A.
N. Akchurin, L. Berntzon, K. Gumus, C. Jeong, H. Kim, S.W. Lee, S. Popescu, Y. Roh, A. Sill, I. Volobouev, E. Washington, R. Wigmans, E. Yazgan

Vanderbilt University, Nashville, U.S.A.
D. Engh, C. Florez, W. Johns, S. Pathak, P. Sheldon

University of Virginia, Charlottesville, U.S.A.
D. Andelin, M.W. Arenton, M. Balazs, S. Boutle, M. Buehler, S. Conetti, B. Cox, R. Hirosky, A. Ledovskoy, C. Neu, D. Phillips II, M. Ronquest, R. Yohay

2010 JINST 5 T03009

Wayne State University, Detroit, U.S.A.
S. Gollapinni, K. Gunthoti, R. Harr, P.E. Karchin, M. Mattson, A. Sakharov

University of Wisconsin, Madison, U.S.A.
M. Anderson, M. Bachtis, J.N. Bellinger, D. Carlsmith, I. Crotty[1], S. Dasu, S. Dutta, J. Efron, F. Feyzi, K. Flood, L. Gray, K.S. Grogg, M. Grothe, R. Hall-Wilton[1], M. Jaworski, P. Klabbers, J. Klukas, A. Lanaro, C. Lazaridis, J. Leonard, R. Loveless, M. Magrans de Abril, A. Mohapatra, G. Ott, G. Polese, D. Reeder, A. Savin, W.H. Smith, A. Sourkov[40], J. Swanson, M. Weinberg, D. Wenman, M. Wensveen, A. White

†: Deceased
1: Also at CERN, European Organization for Nuclear Research, Geneva, Switzerland
2: Also at Universidade Federal do ABC, Santo Andre, Brazil
3: Also at Soltan Institute for Nuclear Studies, Warsaw, Poland
4: Also at Université de Haute-Alsace, Mulhouse, France
5: Also at Centre de Calcul de l'Institut National de Physique Nucleaire et de Physique des Particules (IN2P3), Villeurbanne, France
6: Also at Moscow State University, Moscow, Russia
7: Also at Institute of Nuclear Research ATOMKI, Debrecen, Hungary
8: Also at University of California, San Diego, La Jolla, U.S.A.
9: Also at Tata Institute of Fundamental Research - HECR, Mumbai, India
10: Also at University of Visva-Bharati, Santiniketan, India
11: Also at Facolta' Ingegneria Universita' di Roma "La Sapienza", Roma, Italy
12: Also at Università della Basilicata, Potenza, Italy
13: Also at Laboratori Nazionali di Legnaro dell' INFN, Legnaro, Italy
14: Also at Università di Trento, Trento, Italy
15: Also at ENEA - Casaccia Research Center, S. Maria di Galeria, Italy
16: Also at Warsaw University of Technology, Institute of Electronic Systems, Warsaw, Poland
17: Also at California Institute of Technology, Pasadena, U.S.A.
18: Also at Faculty of Physics of University of Belgrade, Belgrade, Serbia
19: Also at Laboratoire Leprince-Ringuet, Ecole Polytechnique, IN2P3-CNRS, Palaiseau, France
20: Also at Alstom Contracting, Geneve, Switzerland
21: Also at Scuola Normale e Sezione dell' INFN, Pisa, Italy
22: Also at University of Athens, Athens, Greece
23: Also at The University of Kansas, Lawrence, U.S.A.
24: Also at Institute for Theoretical and Experimental Physics, Moscow, Russia
25: Also at Paul Scherrer Institut, Villigen, Switzerland
26: Also at Vinca Institute of Nuclear Sciences, Belgrade, Serbia
27: Also at University of Wisconsin, Madison, U.S.A.
28: Also at Mersin University, Mersin, Turkey
29: Also at Izmir Institute of Technology, Izmir, Turkey
30: Also at Kafkas University, Kars, Turkey
31: Also at Suleyman Demirel University, Isparta, Turkey
32: Also at Ege University, Izmir, Turkey

2010 JINST 5 T03009

33: Also at Rutherford Appleton Laboratory, Didcot, United Kingdom
34: Also at INFN Sezione di Perugia; Universita di Perugia, Perugia, Italy
35: Also at KFKI Research Institute for Particle and Nuclear Physics, Budapest, Hungary
36: Also at Istanbul Technical University, Istanbul, Turkey
37: Also at University of Minnesota, Minneapolis, U.S.A.
38: Also at Institute for Nuclear Research, Moscow, Russia
39: Also at Texas A&M University, College Station, U.S.A.
40: Also at State Research Center of Russian Federation, Institute for High Energy Physics, Protvino, Russia

2010 JINST 5 T03009